Univerza v Mariboru
Fakulteta za energetiko

Journal of ENERGY TECHNOLOGY

Volume 2 / Issue 2
JUNE 2009
www.fe.uni-mb.si/jet

JOURNAL OF ENERGY TECHNOLOGY

VOLUME 2 / Issue 2

Revija Journal of Engineering Technology je indeksirana v naslednjih bazah: - INSPEC©, Cambridge Scientific Abstracts: Abstracts in New Technologies and Engineering (CSA ANTE), ProQuest's Technology Research Database.

Journal JET is indexed and abstracted in following databases: - INSPEC©, Cambridge Scientific Abstracts: Abstracts in New Technologies and Engineering (CSA ANTE), ProQuest's Technology Research Database

JOURNAL OF ENERGY TECHNOLOGY

Tehniška podpora / TECHNICAL SUPPORT

Janko OMERZU
Sonja NOVAK

Izhajanje revije / PUBLISHING

Revija izhaja štirikrat letno v nakladi 300 izvodov. Članki so dostopni na spletni strani revije - www.fe.uni-mb.si/JET .

The journal is published four times a year. Articles are available at the journal's home page - www.fe.uni-mb.si/JET .

Lektoriranje / LANGUAGE EDITING

Terry T. JACKSON

Produkcija / PRODUCTION

Vizualne komunikacije comTEC d.o.o.

Oblikovanje revije in znaka revije / JOURNAL AND LOGO DESIGN

Andrej PREDIN

Prva konferenca ENRE v Sloveniji

Fakulteta za energetiko bo organizirala *Prvo mednarodno konferenco na temo Energetika in Podnebne spremembe* v Velenju, med 1 in 3 julijem 2009. Cilji konference so kako bo Slovenija mogla izvesti načrt, da se doseže 25% delež energije iz obnovljivih virov, da se doseže delež 10% porabe goriv v prometu nadomesti z biogorivi, da se za 20% poveča energetska učinkovitost izrabe primarnih energentov in da se za 20% zniža delež izpustov toplogrednih plinov. Na ta vprašanja bomo v razpravi skušali razjasniti z mednarodnimi strokovnjaki, izmenjati izkušnje, razjasniti marsikatero strokovno dilemo, tudi locirati nova vprašanja in dejstva povezana s klimatskimi spremembami, ter skušali vzpostaviti nove mednarodne znanstvene, strokovne in poslovne povezave. Organizirali bomo okrogle mize na katerih bomo razpravljali in iskali rešitve na ožjih področjih, ki pa bistveno vplivajo na energetske in okoljske dejavnike. Ob konferenci bodo tekle tudi druge spremljevalne dejavnosti, kot so razni ogledi energetskih in premogovniških sistemov, turistični ogledi, ogled mednarodnega atletskega mitinga, ogled svečanega Skoka čez kožo mladih rudarjev, ob njihovem prazniku rudarjev.

Veseli bomo čim širše udeležbe in aktivnega sodelovanja na sami konferenci. Izbrane in ustrezno pripravljene (recenzirane) prispevke bomo objavili v sledečih številkah naše revije JET.

First conference ENRE in Slovenia

Faculty of Energy Technology will organize the *First international conference on Energy and Climate Change* in Velenje, between 1 and 3 July 2009. The objectives of the conference is how Slovenia could carry out a plan to achieve a 25% share of renewable energies to achieve a share of 10% of fuel consumption in transport is replaced by biofuels to 20% increased energy efficiency of utilization of primary energy and that the 20% reduced the proportion of greenhouse gas emissions. In this issue we will try to clarify the debate with international experts to exchange experiences, to clarify the many professional dilemmas, also locate the new issues and facts related to climate change, and seek to establish a new international scientific, technical and commercial links. We will organize round tables on which we will discuss and search for solutions to immediate areas, but significant impact on energy and environmental factors. At the conference they went to other activities such as tours of various energy systems, and coal systems, tourist tours, visit the international athletics meeting, see the ceremony jump through the skin of young miners, on their Day of miners.

We are looking forward and we will be glad to as broad as possible participation and active participation at the conference. Selected and properly prepared (reviewed) contributions will be published in the following numbers of our magazine JET.

Krško, June 2009

Andrej PREDIN

Table of Contents /
Kazalo

JET Volume 2 (2009), p.p. 9 - 18

Issue 2, June 2009

www.fe.uni-mb.si/JET

EXPERIMENTAL AND NUMERICAL APPROACH TO FLOW LOSS ESTIMATION IN A HYDRAULIC PIPE SEGMENT

EKSPERIMENTALNI IN NUMERIČNI PRISTOP K DOLOČITVI TOKOVNIH IZGUB V CEVNEM SEGMENTU

I. BILUŠ[ℜ], R. KLASINC[1], A. PREDIN[2]

Keywords: Numerical modelling, CFD, flow losses, measurements, cavitation;

Abstract

Energy demand is expected to rise in the future and, accordingly, new, optimised solutions should be introduced. This paper presents a study made at the Graz University of Technology analysing the flow losses in the hydraulic pipe junction. The basic idea of the research was to implement modern, computer-based simulation tools and to apply them to the findings of the model tests performed in the laboratory. The goal of present study was to assure the long term cavitation-safe operation of a hydraulic pipe junction with a nozzle.

This paper demonstrates the possibilities and difficulties of using computational fluid dynamics (CFD) in the process of flow loss coefficient determination. The results show that the numerical model with a conventional closure model should be used for the determination of phenomena at the integral point of view.

[ℜ] Dr. Ignacijo Biluš, University of Maribor, Faculty of Mechanical Engineering, Smetanova ulica 17, SI-2000 Maribor, ignacijo.bilus@uni-mb.si

[1] Prof. dr. Roman Klasinc, Graz University of Technology, Institut für Wasserbau und Wasserwirtschaft
Stremayrgasse 10/II, A-8010 Graz, roman.klasinc@tugraz.at

[2] Prof.dr. Andrej Predin, University of Maribor, Faculty of Energy Technology, Hočevarjev trg 1, SI-8270 Krško, andrej.predin@uni-mb.si

---

Povzetek

V prihodnosti se pričakuje, da bodo zahteve po energiji nenehno naraščale, zato se razvijajo nove, bolj optimalne rešitve. V prispevki je prestavljena študija, ki je bila izvedena na Univerzi v Gradcu, ki zajema analizo tokovnih izgub v cevnem priključku oz. na mestu združitve dveh cevovodov. Osnovna ideja raziskav je bila, kako implementirati sodobne metode numeričnega simuliranja tokovnih razmer v takšnem cevnem priključku. Rezultati numeričnih simulacij, pa so verificirani na fizikalnem modelu, oz. so primerjani z rezultati meritev na modelu tekom testiranja modela. Cilj predstavljene raziskave je bil v tem, da se določi meje kavitacijsko varnega obratovanja, v takšnem sektorju združenih cevovodov.

V prispevku so predstavljene možnosti in problemi pri uporabi računalniške dinamike tekočin (CFD) tekom modeliranja toka za določitev koeficienta tokovnih izgub. Rezultati kažejo, da je numerični model s standardnimi (vgrajenimi) možnostmi daje uporabne rezultate pri modeliranju oz. določanju tokovnih izgub, vsaj v integralski obliki.

1 INTRODUCTION

Global demand for all forms of energy is expected to grow in the future. According to long-term forecasts, new power plants will be built and existing systems will be optimised in order to increase the efficiency of energy production.

In the optimisation and construction process, new solutions are frequently introduced and, before their implementation, detailed analyses should be done.

At the Institute for Water Structures and Water Resources Management, at the University of Technology in Graz[3], several research projects were made for different water power plant systems (Kops II, Limberg II) and configurations.

The present contribution introduces the numerical and experimental process used for flow loss estimation at the hydraulic pipe junction with a nozzle.

The basic idea of the research work was to implement modern, computer-based simulation tools (CFD) and to apply them to findings of the model tests performed in the laboratory in the first phase. Then the conclusions were used for extrapolation of results to the nature dimensions with higher Reynolds numbers at the nozzle cross-section in order to assure the cavitation-safe operation regimes.

1.1 The hydraulic pipe junction at Limberg II

The Limberg II pump storage power plant, presently under construction, will use 380 m of height between the existing accumulations: Mooserboden and Wasserfallboden. The new plant will operate in parallel to the Kaprun-Oberstufe pump storage. It is expected that both machines, with power of 240 MW to optimise the system, will increase the total plant power from 353 MW to 833 MW at the turbine operating regime and from 130 MW up to 610 MW at the pump operating regime.

[3] Institut für Wasserbau und Wasserwirtschaft der Technichen Universität Graz

---

The junction geometry at the pressure tunnel-pressure pipe crossing will be manufactured as a choked, double-chamber water column with a nozzle. The advantage of this junction system is in the flow passing chamber (Di=9m) integrated into the water tunnel. The one-armed upper chamber was already defined regarding its position and height, which resulted in a length of 190 m. An additional parameter was the configuration regarding the location and direction of the inclined/diagonal pressure pipe (Di=5.2m) in the continuation of the armoured pressure tunnel (Di=4.8m). The picture below shows a draft of the planned system.

One of the characteristics of the chamber integrated in the water flow, in comparison to a separated one, is the requirement of a stationary flow during simultaneous turbine operation. In order to ensure a free surface flow in a tunnel with a water depth of 4.2m, the declination of the chamber in direction of the pressure pipe was limited to 0.15%. In order to enable ventilation of the chamber for operational purposes, an additional ventilation construction with in-between access from the chamber closure to the upstream pipe was planned.

The Institute of Hydraulic Engineering and Water Resources Management at the University of Technology in Graz performed numerical and physical analyses of junction.

2 FLOW LOSSES ESTIMATION

The pressure losses that occur in hydraulic systems and pipelines due to bends, elbows, joints, valves, etc. are often defined as minor losses. This is a misnomer because in many cases these losses are more important than the losses due to pipe friction. For all minor losses in turbulent flow, the pressure loss varies as the square of the velocity:

$$p_{loss} = \rho \cdot \zeta \cdot \frac{v^2}{2} \tag{2.1}$$

Thus a convenient method of expressing the minor losses in flow is by means of a loss coefficient (ζ). Values of the loss coefficient (ζ) for typical situations and fittings could be found in published literature, while detailed analyses should be made for the special flow segments.

This paper presents two methods for flow loss coefficient estimation at the Limberg II pipe junction nozzle.

2.1 Experimental approach

The pipe junction with nozzle was analysed on physical model with scale of 1:21.8, shown in Figure 1.

The nozzle, its position and flow losses were checked through a hybrid approach; initially through 3D-numerical simulation, and later through a physical model experiment in the ratio of 1:21.8 (s=21.8).

Research on the physical model confirmed the qualitative results of both a numeric calculation as well as the middle flow losses ratio between downstream and upstream equalling 1:2.29.

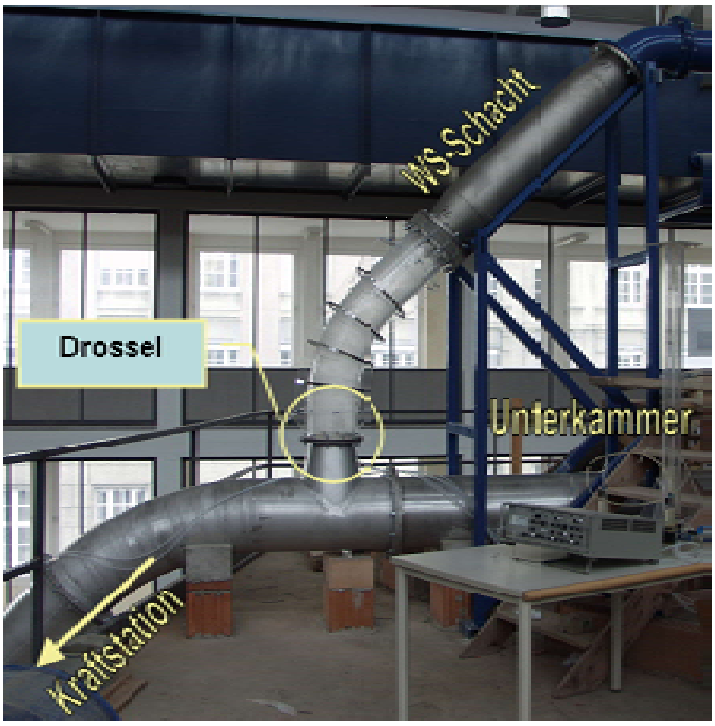

Figure 1: *Pipe junction nozzle model.*

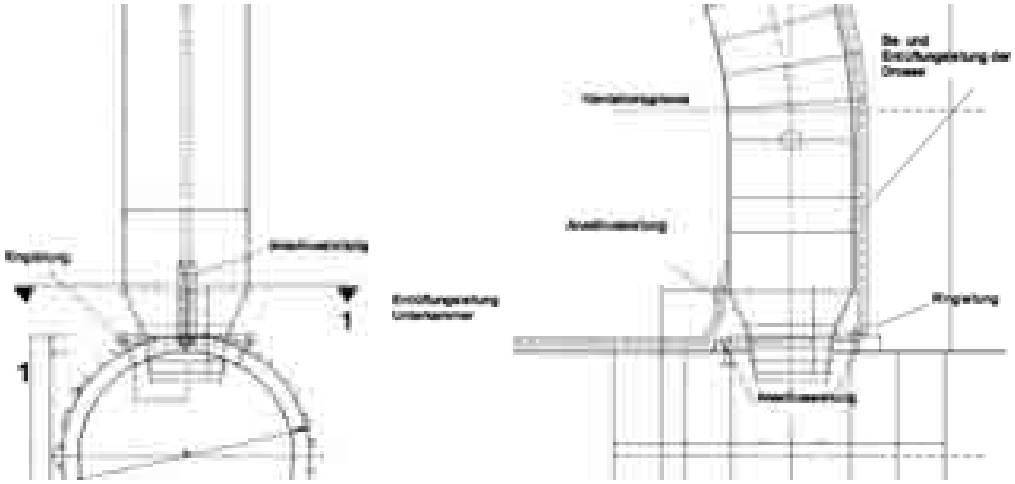

Figure 2: *Pipe junction nozzle details.*

2.2 Numerical approach

Owing to the rapid increase of computer capabilities and according to intensive numerical method development, computational optimisation of hydraulic systems has become possible. In

recent years, CFD has also matured as useful tool in the search for optimal solutions regarding flow behaviour under different operating regimes**Error! Reference source not found.**.

This chapter presents an approach to numerical simulation of water flow through pipe junctions at different scales: from model size (s=1) up to the prototype (life-size) dimension (s=21.8). The analysed scales range indicates the major CFD advantage in comparison to expensive model construction since different scales and Reynolds numbers could be analysed simply and fast.

2.2.1 Computational mesh and boundary conditions

For the presented simulation, unstructured tetrahedral mesh was used. At the junction inlet, static pressure was prescribed and the opening boundary condition with mass flow was defined at the pipe junction exit boundary.

2.2.2 Mathematical model

The conventional Reynolds-averaged Navier Stokes equation system in form of continuity equation, momentum equations and k-e turbulence model was applied for flow simulation. The ANSYS CFX software was used.

2.3 Results

The computational fluid dynamics results for the pump operating regime are shown in Figures 3-6.

Model **Prototype**

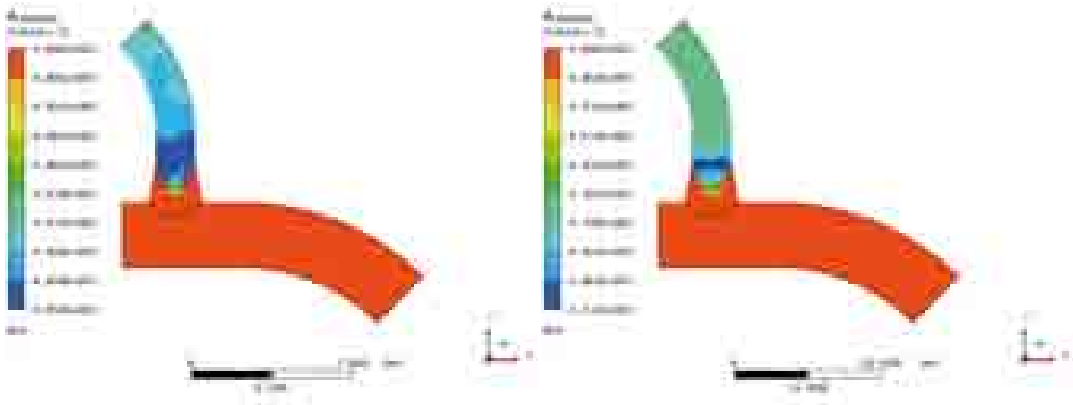

Figure 3: *Pressure distribution for pump operating regime.*

From the results, a comparison for prototype and scale model in the pump operating regime can be made and a reasonable disagreement could be concluded. The reason is in different velocity field (Figure 4), Reynolds numbers and consequently flow regime (turbulence eddy dissipation plots in Figure 6)

Model **Prototype**

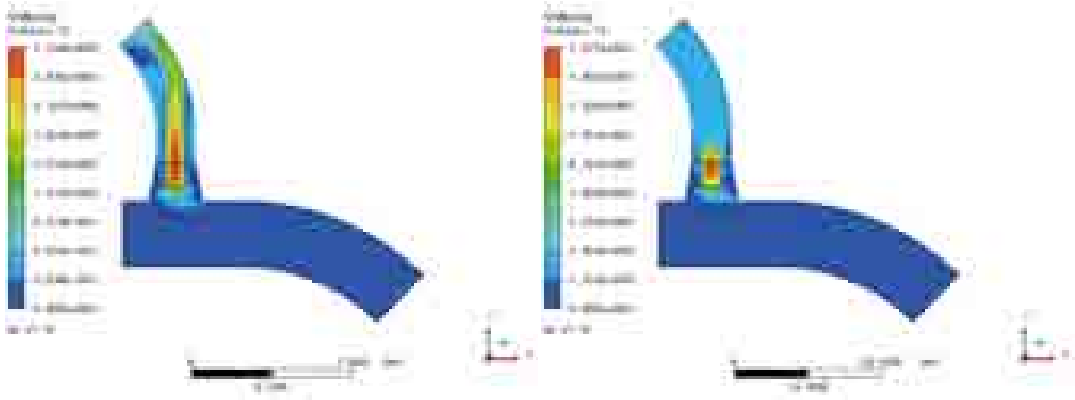

Figure 4: *Velocity distribution for pump operating regime.*

Model **Prototype**

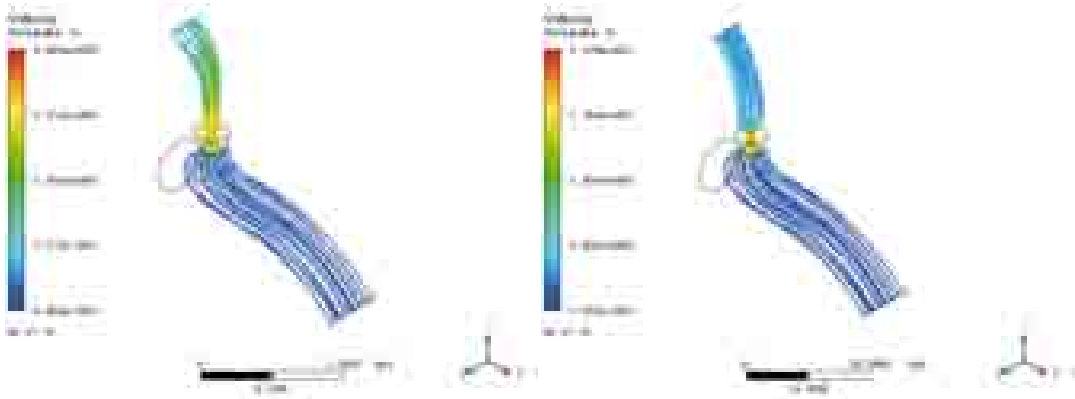

Figure 5: *Streamline plot for pump operating regime.*

Model **Prototype**

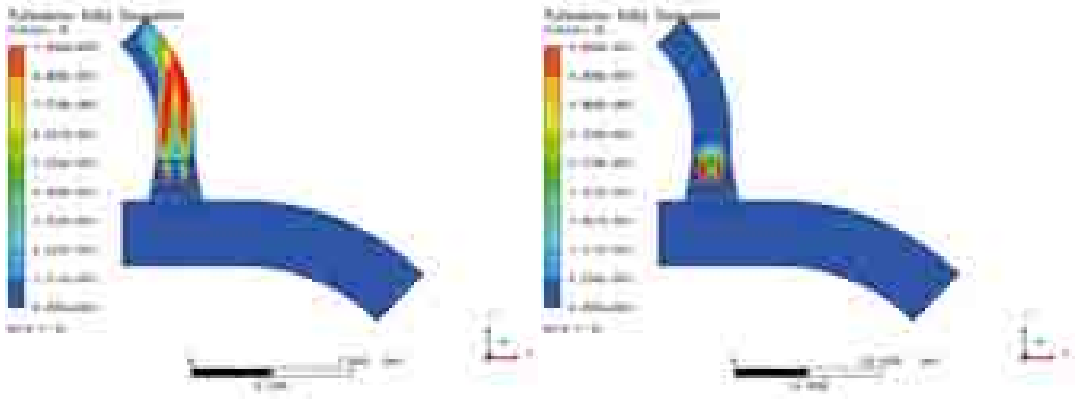

Figure 6: *Turbulence eddy dissipation plot for pump operating regime.*

Model **Prototype**

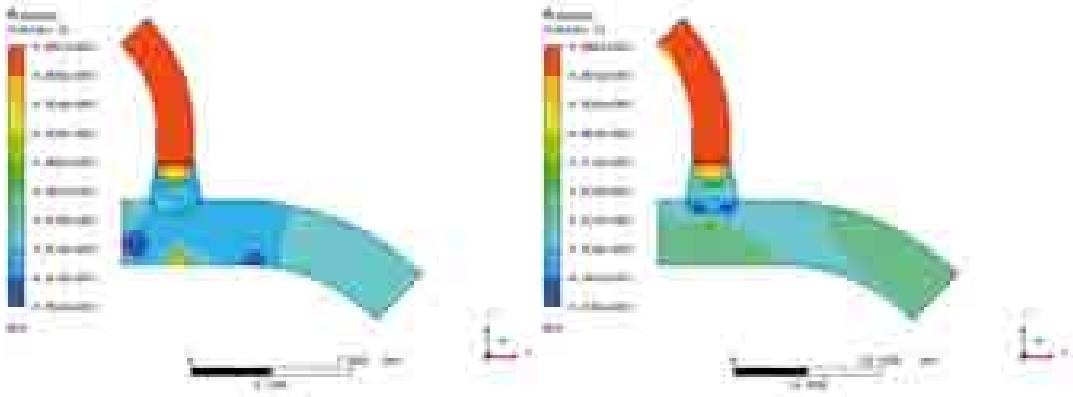

Figure 7: *Pressure distribution for turbine operating regime.*

Model **Prototype**

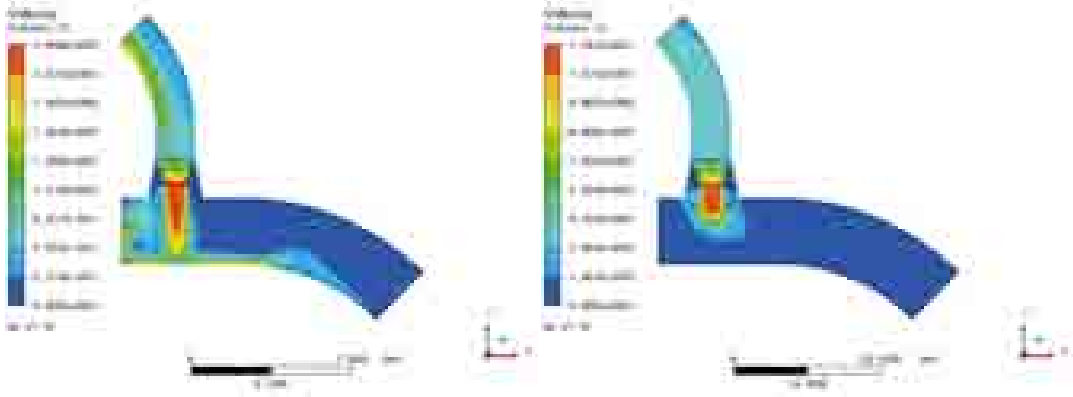

Figure 8: *Velocity distribution for turbine operating regime.*

Model **Prototype**

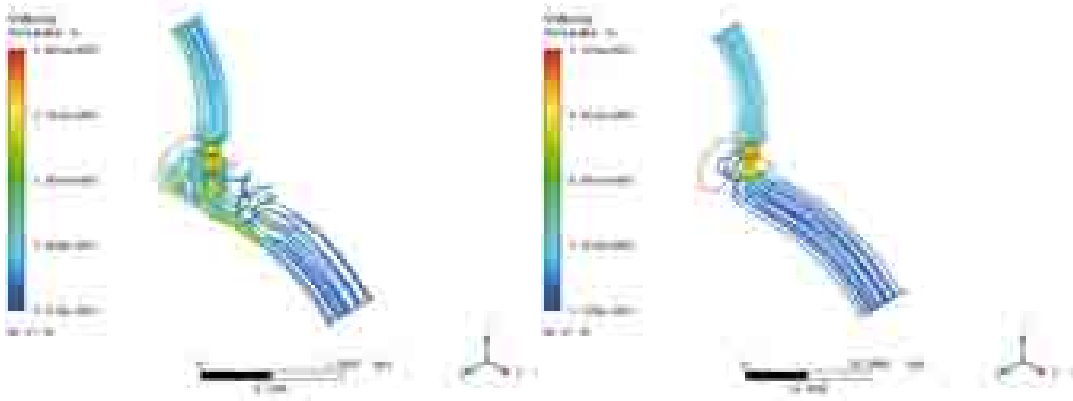

Figure 9: *Streamline plot for turbine operating regime.*

Model **Prototype**

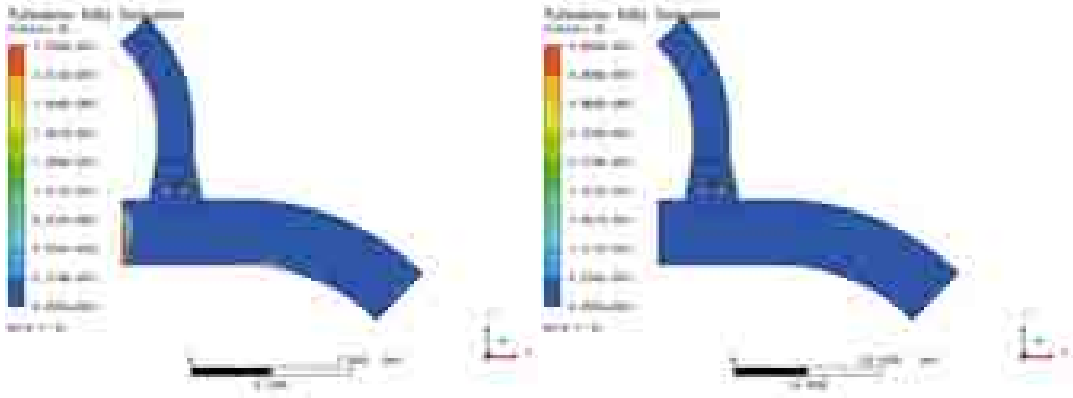

Figure 10: *Turbulence eddy dissipation plot for turbine operating regime.*

The comparison of results for the prototype and scale model in the turbine operating regime confirms the findings from the pump operating regime. The flow pattern distinction is clearly evident at the streamline plots shown in Figure 9.

2.3.1 Flow losses coefficient comparison

According to the relatively good agreement between results at scale s=21.8; the CFD results for different scales was transposed to dependency flow losses-Reynolds number values. The comparison for a variety of operating regimes is shown below.

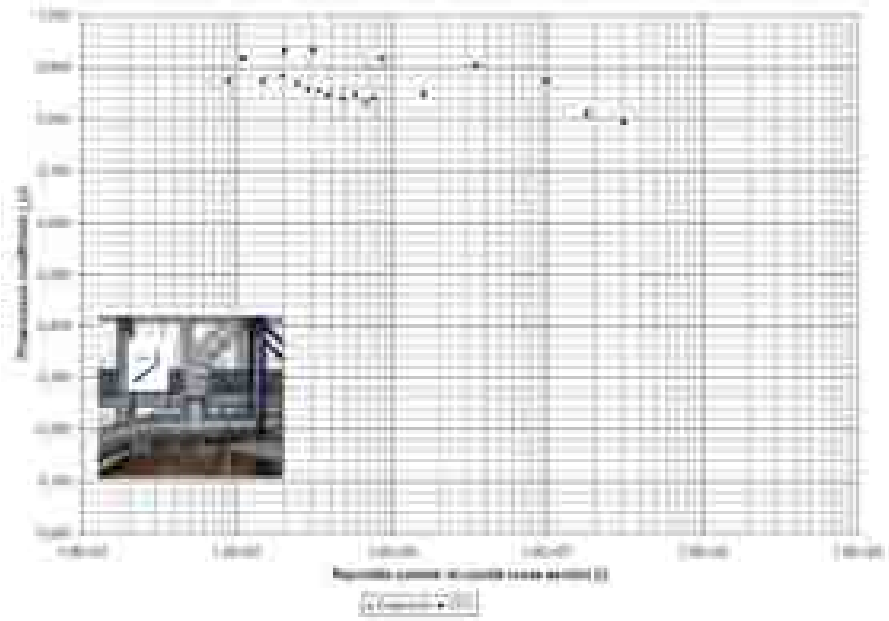

Figure 11: *Results comparison for turbine operating regime.*

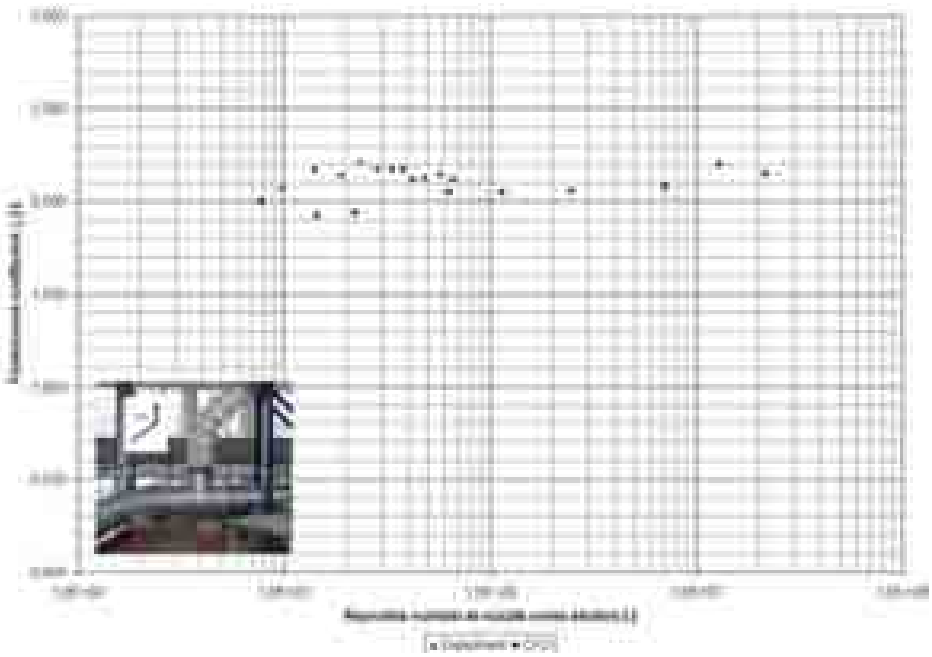

Figure 12: *Results comparison for pump operating regime.*

It is evident from Figures 11 and 12, that the flow loss coefficient follows the experimental results in the area of lower Reynolds number values. According to this, CFD predictions of coefficients at Reynolds number values higher than 1e6 should be assumed to be correct

3 CONCLUSIONS

The present work demonstrates the possibilities and difficulties of using CFD in the process of hydraulic machinery optimisation and flow loss coefficient determination.

The numerical and experimental results for different geometry scales presented in this manuscript show reasonable agreement.

Both results show the same flow loss coefficient distribution along different Reynolds number values.

The results show that RANS numerical model with conventional closure model-transport equations for turbulent kinetic energy and turbulence kinetic energy dissipation should be used for determination of phenomena at the integral point of view.

The computational fluid mechanics results confirm the experimental values with average results deviation up to 15%.

It can be said that the conventional RANS model used is a suitable tool for flow loss coefficient calculation, for the prediction of flow phenomena and as a fast method for geometry optimisation despite to the mismatch comparison to physics (empirical models).

References

[1] [**D. Marjavaara, S. Lundström**, Response surface-based shape optimisation of a Francis draft tube, International Journal of Numerical Methods for Heat and Fluid Flow, Vol. 17, No. 1, Emerald Group, p.p. 34-45, 2007.

[2] **J. Wang, G. H. Priestman, J. R. Tippetts**, Modelling of strongly swirling flows in a complex geometry using unstructured meshes, International Journal of Numerical Methods for Heat and Fluid Flow, Vol. 16, No. 8, Emerald Group, p.p. 910-926, 2006.

[3] **A. Bergant**, Transient cavitating flow in piping systems. Acta hydrotech., Volume 18, Number 29, p.p. 5-17, 2000.

[4] **B. Matijašević, S. Sviderek, T. Mihalić**, Effect of Turbulence Model on Unsteady Flow Simulation, WSEAS Transactions on Fluid Mechanics, No. 5, Vol 1, 2006.

[5] **A. Predin, R. Klasinc, I. Biluš, M. Kastrevc**, Fluid flow conditions in asymmetrical nozzle in discharge pipe system of reversible pump turbine, Proceedings of the 7th Int. Conf. on Hydroscience and Engineering (ICHE-2006), p.p. 123-133, 2006.

[6] **F. M. White**, Fluid Mechanics, Forth Edition, McGraw-Hill International Editions, 1999.

Nomenclature

(Symbols)	(Symbol meaning)
p	pressure
v	velocity
ρ	density
ς	Loss coefficient

JET Volume 2 (2009), p.p. 19 - 40

Issue 2, June 2009

www.fe.uni-mb.si/JET

THE DYNAMICS OF ENERGY PRICE MOVEMENTS ESTIMATING COAL PRICE DYNAMICS WITH THE PRINCIPAL COMPONENTS METHOD

DINAMIKA GIBANJA CEN ENERGENTOV IN OCENA DINAMIKE GIBANJA CEN PREMOGA Z METODO GLAVNIH KOMPONENT

M. FESTIĆ[1], S. REPINA[2], A. KAVKLER[3]

Keywords: energy prices, environmental protection measures, renewable resources, coal prices, economic growth; (JEL classification: C22, C40, C50, Q31, Q40).

Abstract

Demand for energy resources is increasing despite efforts at improving energy efficiency. Coal constitutes one quarter of total primary energy production. The future use of coal depends on environmental protection measures and the Kyoto Protocol. The price of coal is influenced by the price of coal production and preparation technologies, i.e. transportation costs, environmental legislation, the price of coal burning technologies, the price of gas purification, the price of CO_2 permissions or emission coupons, consumption, the price of other energy sources (natural gas and oil) and the liberalization of the electricity markets.

We assessed the influence of prices and the use of other energy sources, environmental measures, energy efficiency and the influence of electricity market liberalisation on coal price movements. Our estimation shows that, if the prices of other energy sources and electricity increase, the price of coal increases. If the use of other energy sources increases, and if the gross uses of industrial waste and renewable resources increase, the price of coal decreases. Environmental protection measures contribute to an increase in coal prices. A higher quotient of energy efficiency decelerates the price of coal. Moreover, the euro (to dollar) appreciation decelerates coal prices.

[1] Prof. Mejra Festić, PhD., Faculty of Economics and Business, University of Maribor; EIPF - Economic Institute, Ljubljana. SLOVENIA. mejra.festic@uni-mb.si; mejra.festic@eipf.si; fax: 00386-2-250-8177.

[2] Sebastijan Repina, BS (econ.)., researcher, EIPF - Economic Institute, Ljubljana. sebastijan.repina@eipf.si.

[3] Alenka Kavkler, PhD., Faculty of Economics and Business, University of Maribor; EIPF - Economic Institute, Ljubljana. SLOVENIA. alenka.kavkler@uni-mb.si.

Povzetek

Povpraševanju po energetskih virov narašča kljub prizadevanjem za izboljšanje energetske učinkovitosti. Premog predstavlja eno četrtino skupne porabe primarne energije proizvodnje. Nadaljnjo rabo premoga je odvisna od ukrepov za varovanje okolja in Kjotskega protokola. Cena premoga je vplival na ceno proizvodnje premoga ter pripravi tehnologij, in sicer stroški prevoza, okoljska zakonodaja, je cena za kurjenje premoga tehnologij, je bila cena plina, prečiščevanja, je cena dovoljenja ali emisijo CO2 kuponi, porabe, cen druge vire energije (zemeljski plin in nafto) in liberalizacijo elektroenergetskega trga.

Mi oceniti vpliv cen in uporabi druge vire energije, okoljske ukrepe, za energetsko učinkovitost in vpliv liberalizacije trga z električno energijo na gibanje cen premoga. Naša ocena kaže, da, če se cene drugih energetskih virov in električno energijo povečuje, je cena premoga poveča. Če z uporabo drugih virov energije poveča, in če je bruto uporabe industrijskih odpadkov in obnovljivih virov povečuje, je cena premoga zmanjša. Ukrepe za varstvo okolja prispevajo k povečanju cene premoga. Višji količnik energetske učinkovitosti določa ceno premoga. Poleg tega je evro (v dolarjih) ocenjena vrednost cene premoga.

1 INTRODUCTION

Industrial growth in developing countries such as China and India constitutes an additional pressure on energy price growth. It is expected that in the next thirty years, the demand for energy will increase by approximately 60%. Two thirds of this increase will stem from needs in developing countries, which is expected to reach 50% of world energy consumption by 2030. Price movements do not exempt any energy resource, because they are – in addition to increased demand – dictated by relatively expensive alternative sources and new technological solutions. Thus, further rises in energy prices can be expected on world markets (Clean Energy 2008).

In the US and Canadian markets, household electricity retail prices are much lower than in European countries, which increased annually by 3 to 5% on average until 2005. In contrast, in all other countries, energy prices began to increase after 2001, with the highest increase noted in Great Britain and Germany. The average prices for industrial consumers in the EU27 are comparable with New Zealand retail prices and are almost twice as high as industrial prices in the US. In Europe, prices in 2007 were the highest in Cyprus and Italy and only slightly lower in Germany, Belgium and the United Kingdom. Last year, the lowest electricity prices for industrial consumers in Europe were found in Latvia and Bulgaria. There are no significant deviations in prices between the old EU15 member states and the average price in the EU27 (Brečevič et al. 2008).

Energy demand is met differently in different world regions, the decisive factor being the natural resources in individual regions. Europe depends on the import of primary resources, thus making nuclear energy an important energy resource. Lately, natural gas has gained importance as a primary energy resource. In the US, a country with one of the highest black coal reserves, such coal is the most important energy resource for generating electricity. Oil and petroleum-product consumption still prevails worldwide, with the present situation likely to remain the same until 2025. World consumption growth has been estimated to 1.9% annually

and by 2025 is supposed to increase from the present 80 million barrels a day to 118 million barrels per day (Energy Security 2008).

In recent years, oil prices have risen considerably: by 80% from April 2007 to July 2008. At the beginning of 2008, prices breached the $100/barrel barrier. When taking account of decreased production in OPEC non-member countries, as well as in Russia, this trend is likely to continue in the future. Natural gas is the fastest growing source of primary energy, for which a 67% increase in consumption is forecast by the year 2025. Prices have been higher than in the 1990s in the previous century for several years and are likely to increase in the coming years (Energy Security 2008).[4]

In the next chapter, we will present an overview of coal resources and prices, the consumption dynamics of coal, and environmental measures. In the third chapter, we present the empirical analysis on the determinants of coal price movement. The goal of this paper is to show the model of coal price dynamics on the basis of relevant determinants. We used the principal components method (PCA) to estimate coal price movements by employing the explanatory variables of electricity prices, consumption, the prices of oil, natural gas and uranium, different environmental measures, energy efficiency, nuclear energy and renewable resource consumption. The implications and results are presented in the last chapter.

2 PRICES, RESERVES AND USE OF COAL

Globally, coal is one of the most important energy sources in the production of primary energy, where it contributes, on average, one fourth of all primary energy. In 2004, the share of coal in global primary energy consumption amounted to 27%, in 2005 to 25% (WCI, 2007). By 2030, according to estimates, approximately 39-40% of global electricity requirements will be produced by coal (Lajevec et al. 2007). Thus, coal is likely to remain an important energy resource in the future.

Coal price movements during the last decades can be compared with the movements of oil and natural gas prices, but with regard to energy content, the dynamics are on a substantially lower level.

According to Eurocoal data given in Figure 1, global coal price movements depend on the quality and purpose of various types of coals. According to the standard international qualification of coals Antwerp - Rotterdam - Amsterdam (cif ARA), appropriate quality coal has an energy content of 6000 kcal/kg (29.31 MJ/kg), 1% sulphur content and 16% ash content. The price of coal depends on its quality, where much depends on its calorific value, sulphuric content and the level of moisture.

In comparison with reserves of natural gas and oil, the reserves of coal are much higher and the distribution of reserves, especially black coal, is much more even than the distribution of oil and natural gas. Russia has a considerable share of the global reserves of coal, with important deposits of black coal in North America, Asia, Australia and South Africa, where there is less oil

[4] One MMBtu (MMBtu - million Btu, British thermal unit; 1000 cubic meters of natural gas equals approximately 1MBtu, which is roughly equivalent to 1 GJ) of natural gas produces six times less thermal energy than a barrel of oil (Eurostat 2007). The price of both energy sources maintained a long-term relationship of around 10:1, and is likely to decline to around 7.5:1 (Hartley et al. 2007).

---

and natural gas. The countries with the largest coal reserves include: the USA, Russia, China, India and Australia (75% of proven reserves are found in these countries). In contrast to the reserves of oil and natural gas, there are large deposits of coal in the EU, but with substantial differences in its quality (Lajevec et al. 2007). Data about coal reserves in OECD countries, EU states and in the countries of the former Soviet Union are given in Table 1.

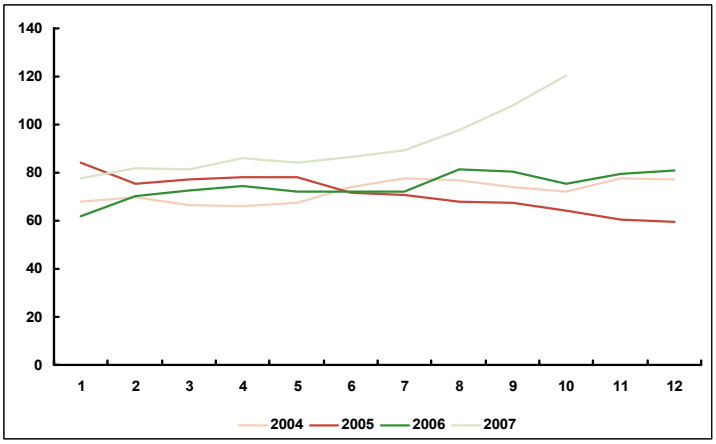

Figure 1: *World monthly prices[*] of energetic coal cif ARA ($/t)* *Prices given in Eurocoal's Market report (1 - 2006, 1 - 2007, 3 - 2007). Source: Eurocoal, http://euracoal.be/newsite/report.php (2008b).

Table 1: *Reserves of coal at the end of 2006*

(mio t)	Anthracite and bituminous coal	Sub-bituminous coal and lignite	Total	Share of total reserves
EU 25	17424	17938	35362	3.9%
EU 27	17450	20593	38043	4.2%
OECD	172363	200857	373220	41.1%
Former Soviet Union	94513	132741	227254	25.0%
Others	211895	96695	308590	33.9%
GLOBAL TOTAL:	478771	430293	909064	100.0%

Source: Statistical Review of World Energy, http://www.bp.com/statisticalreview (2008).

The World Energy Council (WCI 2008) report for 2007 states that world reserves at the end of 2005 amounted to 847.5 Gt, which is 61.5 Gt or 6.8% less than at the end of 2002 (WCI 2007). Taking into account global consumption for 2004, proven reserves of black coal will last for 172 years, and the reserves of brown coal for 218 years.

In Europe, the demand for coal, which on average amounted to around 770 million tons annually, has not changed considerably in recent times. In 2007, in comparison to 2006, the demand slightly decreased. In the first half of 2007, total coal consumption was 398.4 million tons, of which slightly more than one fourth was imported. In the period between 2003 and 2007, there was a trend of reduced consumption of coal in the USA, especially in the commercial sector and households, except in the production of electricity, where consumption increased by 4% (EIA 2007).

In 2005, 16% of global electricity production was generated by hydroelectric power stations, 15% from nuclear power stations, 20% from natural gas, 7% from oil and 40% from coal (WCI 2007, http://www.worldcoal.org). The share of electricity produced from coal varies. In Poland and South Africa, this share exceeds 90%. In Israel, Kazakhstan, India, China and Morocco it constitutes up to 70%. Coal will continue to have the most important role in the production of electricity in the future. Projections until 2030 show an only 1% decrease in coal-powered electricity, which means that its share will remain at 39% (EIA 2008).

On average, the EU uses one fifth of domestic black coal, the consumption of which decreases by 1-2% a year. The deficit in the EU is covered by imports (roughly one third).[5] More than one half of the demand is covered by lignite, which, due to the market situation, became more competitive at the end of 2006 and the beginning of 2007. The consumption of lignite in the EU increased slightly during this period: from 48% of total consumption in 2005, its share increased to 53% of total consumption in the first half of 2007. The reasons for this were to be found in the relatively high price of natural gas and surplus of emission coupons, which reached a price lower than 10 EUR/t CO_2 in October 2006 (at the beginning of 2007 the price of coupons decreased to around 1 EUR /t CO_2) (Eurocoal 2008, 2008a).

2.1 Environmental measures influencing the consumption and price of coal

Future coal reserve consumption depends, and is conditional, on environmental requirements. The price of coal is influenced by the price of coal production and preparation technologies, i.e. transportation costs, environmental legislation, the price of coal burning technology, the price of gas purification, the price of CO_2 permissions or emission coupons, the consumption and price of other energy sources (natural gas and oil) and liberalization of the electricity markets. Forecast emissions of CO_2 are increasing until 2030 due to increased energy consumption (Kucewitz 2007).

Coal mining has numerous environmental impacts, especially in the case of surface mining on large areas of land that may become permanently degraded, and are subject to soil erosion, dust, noise, the creation of waste waters and leachate, as well as damaging local biodiversity. In underground mining, methane (CH_4) is released, a greenhouse gas emission (GHG). Around 8% of global methane emissions are due to coal burning, of which China, Russia, Poland and the United States account for over 77 % of coal mine CH_4 emissions (WEC 2008).

The consumption of coal causes further environmental stress because of CO_2 emissions, sulphur oxides (SO_x) and nitrogen oxides (NO_x) responsible for acid rain, and flying ash, which includes

[5] Germany is the biggest coal consumer in the EU. Together with the UK, Germany is also the biggest black coal importer.

---

dust particles and heavy metals, particularly mercury (Hg) and selenium (Se). In addition, the effects of coal mining and burning include the emission of toxic substances in soil, surface water and indirectly into groundwater.

Environmental issues influencing the consumption and price of coal can thus be summarised as follows: mining technologies, transportation, the preparation and combustion procedure, technology gas purification, all of which have the main aim of improving coal efficiency with the lowest possible emissions of dust, CO_2,SO_2 in NO_x (WCI 2004). Due to these environmental issues, different technologies are being developed in order to improve combustion that, as already noted, consumes 40% of global coal production.

Iceland	Australia**	Norway	New Zeland	Croatia	Canada	USA	EU 15
			Rusia		Hungary		Bulgaria
			Ukraine		Japan		Czech Rep.
					Polan		Estonia
							Latvia
							Liechtenstein
							Lithuania
							Monaco

Figure 2: *Emission targets according to Kyoto Protocol (1990* - 2008/2012),* Source: The Coal Resource, WCI (2007).

Coal CO_2 emissions are similar to those of other fossil fuels (21% natural gas, 38% coal and 41% oil). In order to reduce emissions, the Kyoto Protocol was adopted in 1997, which entered into force on February 16, 2005 (WCI 2004). Figure 2 shows data on emission targets for different countries.

According to *The Coal Resource* – published by the World Coal Institute (WCI 2007) – CO_2 emissions from coal in the EU amounted to 1.275 Mt. According to the Energy Information Administration, the emissions amounted to 1.356 Mt (EIA 2007). Table 2 shows the emissions of CO_2 by continent. It can be seen that Europe managed to reverse its emissions trend. The USA succeeded in doing the same in 2006; in contrast, Asia and the Pacific area have seen a 10 percent annual increase.

The Kyoto Protocol also introduced emissions trading with the so-called emission coupons, which became the key mechanism in efforts to reduce GHG emissions. The USA and Australia did not ratify the Kyoto Protocol, but they implemented their own measures in order to reduce emissions. Below are the main features of the European emission trading schemes (EU-ETS) (Table 3).

Table 2: *CO_2 emissions from coal in 2003 -2006 (10^6 t),* Source: EIA (2008).

Area	2003	2004	P2005	P2006
North America	2,277.96	2,294.31	2,330.00	2,300.96
Middle and South America	73.22	77.86	80.51	-
Europe	1,372.35	1,376.33	1,355.71	-
Eurasia	694.20	677.40	693.71	-
Middle East	33.89	34.55	35.44	-
Africa	364.66	394.14	385.51	-
Asia and Oceania	5,090.71	5,909.17	6,476.32	-
Global:	9,906.99	10,763.75	11,357.19	-

P ….preliminary data

- …..no data

Table 3: *Key features of the EU emissions trading scheme (EU-ETS), Source: Reinaud (2007).*

Features	Description
Target	One allowance in the EU-ETS allows the owner to emit 1 tonne of CO_2 equivalent; its validity is limited to a specific period. During 2005-2007, a mostly free allocation of coupons.
Allocation mode	Up to 5% auctioning allowed during 2005-2007. Up to 10% auctioning allowed for 2008-2012.
New entrants	Each member state decides about the way and quantities of access allowances.
Plant closure	Member states shall decide whether allowances should be surrendered or kept after closure (likewise, the decision about the transfer of allowances to a new facility is to the discretion of each member state).
Penalties	A penalty tax of 40 EUR per tonne for excess CO2 emissions in the first compliance period and of 100 EUR in the second period, plus restoration of the GHG emitted without having surrendered allowances.

Emissions trading have had a huge impact on the European energy market. When the emission trading system was introduced, it involved around 11,500 plants across the EU25. It is based on the exchange of unused emission allowances, with 14.6 billion EUR transactions in 2006 (Reinaud 2007). In OECD countries, the largest participants in emission trading are thermal

power plants, which represent 50% EU-ETS in the EU. Within the first trading period, the relationship between the prices of emission coupons, the price of electricity and industrial expenses was established. Figure 3 illustrates the price movements of emission allowances for 2003-2006 in the EU-ETS.

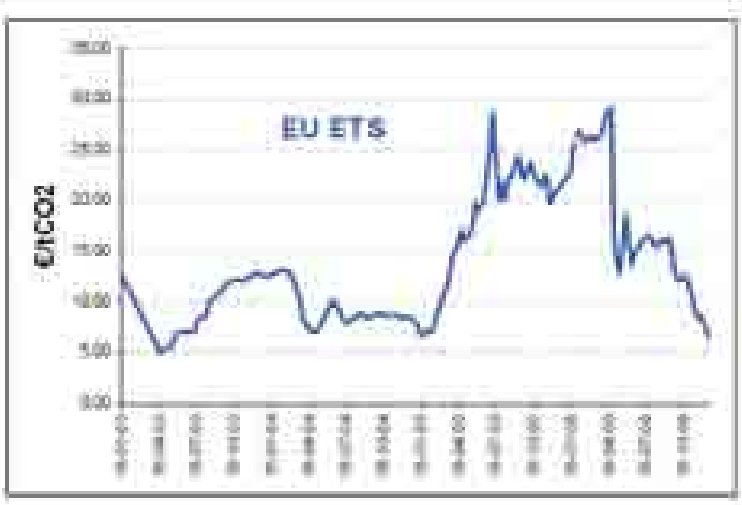

***Figure 3*:** Price movements of emission coupons in the European emissions market, Source: Reinaud (2007).

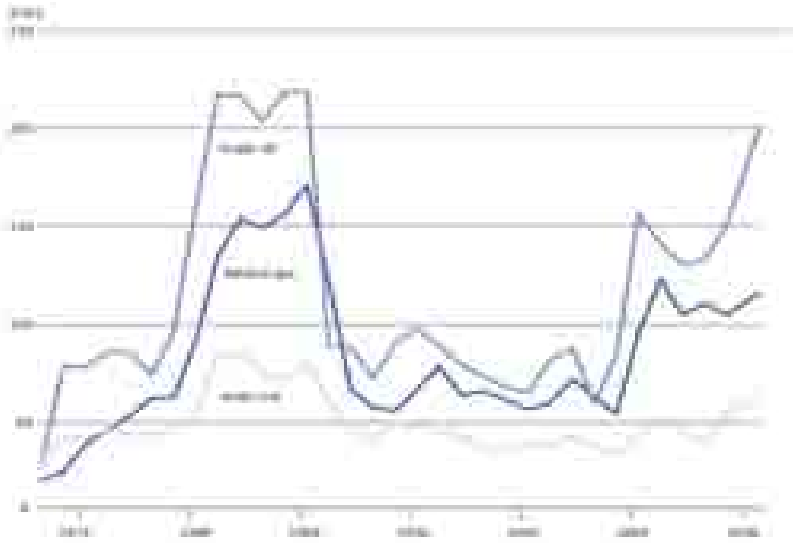

Figure 4: *Price movements of fossil fuels in the EU, Source: Eurocoal, http://euracoal.be/newsite/world_market_hard_coal.pdf (2007a).*

The countries with the largest thermal power plants (Germany, Estonia, and Poland, as well as Slovenia), which also use coal, usually dictate the basic electricity price. In comparison with

other fossil fuels, coal is relatively cheap, as shown in Figure 4. New carbon capture and storage technologies (Carbon Capture and Storage - CCS) will increase the range of possibilities for coal use within the coming decades (Eurocoal 2007).

Until 2030, the price of electricity is likely to increase due to increased demand, expensive energy and capital intensive technologies and reach 58-73 EUR/MWh (Brečevič et al. 2008). Such estimates take into account prices for emission coupons ranging from 2 EUR to 12 EUR/t CO_2ekv.

The use of coal in the EU will also be influenced by the price of natural gas and emission coupons. If natural gas is relatively expensive, it will only be competitive when the price of emission coupons exceeds 30 EUR/t CO_2ekv. In order to decrease emissions, the price of coupons should be at least 45 EUR/t CO_2ekv. If the price of natural gas is low, coal will only be competitive on the liberalised energy market if the price of coupons is lower than 15 EUR/t CO_2ekv. Estimates in studies show (Kavalov and Peteves 2007, Eurocoal 2007b) that the use of coal on the liberalized European energy market will remain competitive in the next twenty years in highly efficient thermal power plants by implementing CCS technologies. This is done on the assumption that the price of emission coupons will remain slightly below 30 EUR/t CO_2ekv (Eurocoal 2007b).

In 2008, the price of emission coupons was decreasing. The price on January 1, 2008, was 5.53 EUR but dropped to 2.00 EUR by December 28. The price of coupons on the free market was around 1.00 EUR by the end of March 2008, which, according to the opinion of some experts, equals zero (EEX 2008). How the price will move in the new 2008-2012 trading period, which will try to correct some mistakes from the first trading period, is difficult to forecast. According to some estimates, the price of emission coupons is likely to be higher, because there will not be so many coupons available. During this period, the price was likely to be in the range of 20 to 21 EUR/t CO_2ekv (Energy 2008).

3 COAL PRICE DYNAMIC FACTORS

Methodology: In order to assess the influence of individual explanatory variables on coal price movements, we used the least squares method (OLS regression) by employing principal components (PCA). Models were assessed on quarterly data within the period from the first quarter of 1995 until the fourth quarter of 2007. EIPF, IRRET, OECD and EUROSTAT (2008) databases were used.

We assessed the influence of prices and the use of other energy sources, environmental measures and the influence of electricity market liberalization on the movement of coal prices.[6] By implementing the method of Principal Components Analysis (PCA) (Harris 1997), the amount of data or explanatory variables was narrowed (see: Table A, Appendix). The PCA method explains the variance-covariance structure of the investigated variables by introducing some additional new variables, which present the linear combination of the primary variables, and are known as principal components (Fuentes and Godoy 2005). An analysis of principal components often reveals relationships that were not previously suspected and thereby allows interpretations that would not ordinarily appear (Rao 1964). The main advantage of PCA is that

[6] The price of coal is given as import price in EUR/t (OECD, 2008). The price of coal is the average price for all types of coal imported into the EU25.

---

once these patterns in the data are found, and the data is compressed, i.e. by reducing the number of dimensions, there is no serious loss of information (Favero et al. 2005). By obtaining the eigenvector (component) with the highest eigenvalues, the principle component of the data set is obtained (Wetzstein and Green 1978). Once the components (eigenvectors) are chosen that to be kept in the data and form a feature vector, the transpose of the vector is simply taken and multiplied on the left of the original data set, transposed (Harris 1997). The final data is the final data set (Rovan 2006, Baxter et al. 1990).

The principal components analysis can either be done on raw or mean-corrected data on one hand or on standardized data on the other. The influence of an individual variable on principal components is determined by the magnitude of its variance. The higher the variance of the variable, the stronger the effect of a variable on principal components. In the case of standardized data, the basis for principal component analysis is a correlation matrix. All the variances are equal to one and therefore they all have the same influence on principal components. In cases where there is a reason to believe that the variances of the variables indicate the importance of a given variable and the units of the measure are commensurable, the raw or the mean-corrected data should be used (Rovan 2006, Graffelman and Aluja-Banet 2003). In all other cases, standardized data constitutes a preferable alternative (Kaciak and Koczkodaj 1989, Rovan 2006). In order to find the number of principal components, we could use Kaiser's rule. Standardized data suggests only retaining those components whose eigenvalues are greater than one. The rationale for this rule is that for standardized data, the amount of variance extracted by each component should, at a minimum, be equal to the variance of at least one variable (Cattell, 1966).

The interpretability of the principal components is used in deciding on how many principal components should be retained (Sharma 2000). Since principal components are linear combinations of the original variables, one can use correlations between the original variables and principal components for interpreting principal components. The higher the loading of a variable, the more influence it has in the formation of the principal component score (a loading of 0.5 or above is used as a cutoff point) (Rao 1964).

Data: For the explanatory variable on the use of other energy sources, we merged a time series for gross domestic electricity consumption, gross domestic renewable energy sources consumption (wind power, biomass, photovoltaic cells and hydro energy) and industrial waste, gross domestic crude oil and petroleum products consumption, natural gas and nuclear energy (for the EU25, in kTOE).[7] We used the principal components for interpretations instead of the original variables due to the substantial amount of total variance in the data set, which was accounted for by a few first principal components. From six variables, we arrived at three vectors, or explanatory variables, with an explanatory power of 95.4% variance of basic explanatory variables. The explanatory variable for the price of other energy sources includes the price of oil, natural gas and uranium.[8] From the above-mentioned three energy prices, we arrived at the explanatory variable with an explanatory power of 90.4% variance of basic explanatory variables. Because the price of coal depends on dollar exchange rate fluctuations, we used the dollar-euro exchange rates as an additional explanatory variable.

[7] TOE is a unit of oil equivalent, which is the amount of energy released by burning one tonne of crude oil. Toe is a unit used mainly to show the use of energy in energy balances. 1000 toe = 41,868 TJ.

[8] Natural gas price is given in EUR/Mbtu as a weighted average of import prices for the EU25. The price of oil is in EU/barrel (brent). The price of uranium is in EUR/kg of uranium.

The following variables were used as explanatory variables for environmental measures: industrial air pollution (CO, CO_2 and SO_X in 1000 tons), expenses for environmental protection in all industries within the EU25 (1000 EUR), the share of renewable energy resources in primary energy production (in kTOE), taxes on environment pollution (in millions of euros) and gross domestic consumption of renewable energy resources (in kTOE). Thus, we arrived at three new explanatory variables with an explanatory power of 93.4% variance of basic variables.[9]

The explanatory variable for the price of electricity (in EUR/MWh) explains the influence of electricity market liberalisation. Due to the positive correlation between the price of electricity and the export or import of electricity (0.365/0.366), imports and exports were not included in the regression. Due to the strong positive correlation between the export and import of electricity (with a coefficient of 0.981), it can be concluded that the security of electricity supply is important in a different time-scale. Energy efficiency was used as the second explanatory variable for the explanation of the liberalization of the electricity market (as a ratio between the available amount of energy for consumption and gross domestic consumption).

Estimation and results: The regression equation is estimated with a logarithm difference (dlog) of chosen variables and by taking into account the optimal time lag and best Akaike criterion. We calculated the presence of a common square (H_0 = common square) in variables. The augmented Dickey-Fuller test (ADF) for chosen variables (in dlog form) refuted the hypothesis regarding the existence of the common square, because ADF values exceeded critical values with a 1% degree of significance (Dickey and Fuller 1979). The applied time series were standardized in order to match units, in which some time series are given.

The statistical significance of the coefficients of regression equations was accepted when response variables had P-values lower than 0.05. The Breusch-Godfrey test was used to check the hypothesis behind the existence of the serial autocorrelation of residuals; due to the good results of the Breusch-Godfrey test (low F-statistics and high P-values, see: Table 4), we accepted the hypothesis H_0 about the non-existence of the serial autocorrelation of residuals (Breusch 1979).[10] We had appropriate adequacy criterion for the equation R^2 (Table 4) and the normality test (see Appendix, Table B). The stability of the chosen model was confirmed with the Ramsey-Reset stability test (Ramsey 1969), which has given us good results with low F-statistics values and a high P-value (see: Table 4). According to the Chow forecast test (Table 4), which was used for proving the stability of the estimated functions, we accepted the hypothesis regarding structural stability (Thursby 1982). The regression was analyzed on the basis of the following model:

$$Dlog(P\_coal\_et)_t = b_1 \cdot Dlog(FAC1\_2)_{t-4} + b_2 \cdot Dlog(FAC2\_2)_{t-4} + b_3 \cdot Dlog(FAC3\_2)_{t-4} + b_4 \cdot Dlog(FAC1\_4)_{t-1} + b_5 \cdot Dlog(FAC1\_1)_{t-1} + b_6 \cdot Dlog(FAC2\_1)_{t-1} + b_7 \cdot Dlog(FAC3\_1)_{t-1} + b_8 \cdot Dlog(G\_Electricity)_{t-3} + b_9 \cdot Dlog(energy\_effici)_{t-3} + b_{10} \cdot Dlog(exch\_r)_t + \varepsilon_t$$

where Dlog represents the logarithm difference, b_x the coefficient of regression equations, FAC1_2, FAC2_2 and FAC3_2 the main components of the consumption of other energy source variables, of which coefficients are aggregated ($b_1+b_2+b_3$), FAC1_4 as the main component of the energy price variable (with b_4 coefficient), while FAC1_1, FAC2_1 and FAC3_1 are the main

[9] Variables were standardized.

[10] Equally good results were arrived at by using correlograms. The Q-Statistics (Appendix, Table C) were employed to check autocorrelation in residuals. We accepted the hypothesis of no autocorrelation of residuals: with high probabilities and low Q-statistics.

---

components of the environmental measures variable, of which coefficients are aggregated (b_5+b_6+b_7), G_electricity is a variable for the price of electricity, "energy_effici" is a variable for the quotient between the available energy for final consumption and gross domestic consumption and "exch_r" is the variable for the dollar-euro exchange rate, and ε_t is the error term.

Table 4: *Regression estimates for factors influencing coal price movements.*

Dependent Variable: DLOG(P_COAL_ET) Method: Least Squares, n=52				
	Coefficient	Std. Error	t-Statistic	Prob.
DLOG(FAC1_2(-4))	-1.551347	0.244672	-6.340506	0.0000
DLOG(FAC2_2(-4))	0.381896	0.089121	4.285158	0.0001
DLOG(FAC3_2(-4))	-0.914823	0.155957	-5.865877	0.0000
DLOG(FAC1_3(-1))	0.611380	0.203826	2.999528	0.0048
DLOG(FAC1_1)	1.870693	0.333605	5.607513	0.0000
DLOG(FAC2_1)	-0.233555	0.110978	-2.104515	0.0422
DLOG(FAC3_1)	-0.058241	0.085520	-0.681022	0.0874
DLOG(G_ELECTRICITY(-3))	0.387955	0.169635	2.287004	0.0280
DLOG(ENERGY_EFFICI(-3))	-0.322184	0.139892	-2.303101	0.0270
DLOG(EXCH_R)	-0.546229	0.070890	-7.705335	0.0000
Breusch-Godfrey Serial Correlation LM Test: F-statistic = 0.002432 (Prob. F(1, 36) =0.9609), F-statistic = 1.126017 (Prob. F(3, 34) =0.3523). Ramsey Reset Test: F-statistic = 0.216592 (Prob. F(1, 36) =0.6445); F-statistic = 0.224476 (Prob. F(2, 35) =0.8001); F-statistic = 1.265623 (Prob. F(9,28) =0.3981). Chow Forecast Test: Forecast from 1999:1 to 2007:4, F-statistic = 4.796227 (Prob. F(1, 36) =0.3493).				
R-squared	0.754391			
Adjusted R-squared	0.694648	Mean dependent var	0.011372	
S.E. of regression	0.053198	S.D. dependent var	0.096270	
Sum squared resid	0.104710	Akaike info criterion	-2.843301	
Log likelihood	76.81757	Schwarz criterion	-2.449653	
Durbin-Watson stat	1.562021	Hannan-Quinn criter.	-2.695168	

Optimal time lags in regression were calculated by taking into account the Akaike criterion. The use of other energy influences the dynamics of coal prices with a time lag of four quarters. The dynamics of coal price movements respond to the dynamics of price movements of other energy sources with a time lag of one quarter and to the dynamics of electricity price movements and energy efficiency with a time lag of three quarters. Environmental measures and the influence of the exchange rate influence coal prices in the same quarter (Table 4).

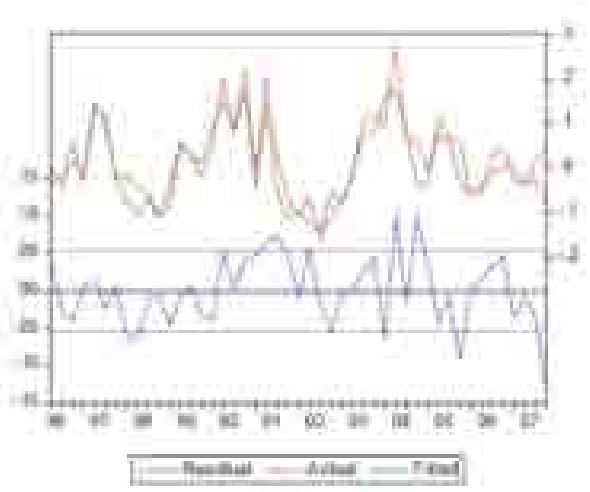

Figure 5: *Actual and estimated values of dependent variables*

Due to the standardised data, we will discuss the results in the following way: a 1% change of standard deviation of constituent components of the main component or dependent variable is multiplied by the coefficient (b_x) and the st. dev. of the coal price. Alternatively, the obtained values can be transformed with regard to a coal price change of one EUR/t.

If the prices of other energy sources increase, i.e. if crude oil price is increased by 1.962 EUR/barrel, the price of natural gas by 0.172 EUR/Mbtu and the price of uranium by 0.332 EUR/kg, the price of coal increases by 0.531 EUR/t (ceteris paribus). Or, if the price of other energents increases so that the price of crude oil increases by 3.695 EUR/barrel, the price of natural gas by 0.323 EUR/Mbtu and the price of uranium by 0.625 EUR/kg, then the price of coal increases by 1.00 EUR/t (ceteris paribus).

If the consumption of other energents increases so that the gross domestic electricity consumption increases by 8.789 kTOE, gross domestic consumption of industrial waste by 7.439 kTOE, gross domestic consumption of renewable resources by 139.486 kTOE, gross domestic consumption of crude oil by 88.533 kTOE, gross domestic consumption of natural gas by 402.542 kTOE and gross domestic consumption of nuclear power by 115.052 kTOE, the price of coal decreases by -0.181 EUR/t. Or if the consumption of other energy sources increases so that the gross domestic consumption of electricity increases by 48.583 kTOE, gross domestic consumption of industrial waste by 41.121 kTOE, gross domestic consumption of renewable resources by 771.065 kTOE, gross domestic consumption of crude oil by 489.402 kTOE, gross domestic consumption of natural gas by 2,225.218 kTOE and gross domestic consumption of nuclear energy by 635.998 kTOE, the price of coal decreases by -1.00 EUR/t.

Environmental measures contribute to (cumulative) rising prices for coal. If the energy industry contributes to air pollution by 0.504 kt CO, 351.865 kt CO_2 and 18.345 kt SO_x, and if the environmental protection costs in the whole industry sector within the EU25 increases by 40.884 million EUR, the share of renewable resources consumption in primary energy production by 108.375 kTOE, taxes on environment pollution by 23.644 million EUR and gross domestic renewable resources consumption by 139.486 kTOE, then the price of coal increases by 0.137 EUR/t. Or if the energy industry contributes 3.678 kt CO, 2,566.487 kt CO_2 and 133.810 kt SO_x to air pollution and if the cost for environment protection in the whole industry within the EU25 increases by 298.206 million EUR, the share of renewable sources consumption in primary energy production by 790.482 kTOE, taxes on environmental pollution by 171.456 million EUR and gross domestic consumption of renewable sources by 1,017.400 kTOE, the price of coal increases by 1.00 EUR/t.

The price of electricity causes an increase in the price of coal. If the price of electricity increases by 0.0606 EUR/MWh, the price of coal increases by 0.0337 EUR/t, or the price of electricity increases by 1.799 EUR/MWh contributes to a price of coal increase by 1.00 EUR/t.

The increase of the energy efficiency quotient by $4.48 \cdot 10^{-5}$ decreases the price of coal by -0.028 EUR/t. The increase of the energy efficiency quotient by 0.002 decreases the price of coal by -1.00 EUR/t.

The increase in the dollar-euro exchange rate decreases the price of coal. If the dollar-euro exchange rate (EUR appreciation) increases by 0.00153, the price of coal decreases by -0.047 EUR/t. Conversely, if the dollar-euro exchange rate (EUR appreciation) increases by 0.032, the price of coal decreases by -1.00 EUR/t.

3.1 Coal price movement forecast

Methodology: On the basis of real data about coal prices for the period from 2002:01 to 2007:04, we carried out linear regression by taking into account the trend of coal price movements in the stated period. The time prior to the stated period was excluded from the regression because of the different dynamics in coal price movements. With the implementation of the Chow Breakpoint test (Appendix, Table D) we defined the breakpoint year as 2002 (see: Figure 6).

On the basis of the real values of explanatory variables from the model in Table 4, we implemented linear regression with the breakpoint year as 2002. The anticipated values of explanatory variables were used in the model given in Table 4 and forecast coal price movements in the existing model until 2032 (see: Figure 7).

Results: The forecast for coal price movements on the basis of our model from Table 4 shows a substantial increase after 2008 with the breakpoint year 2023, when the growth trend strengthens. From 2009 to 2020, the price of coal is likely to increase from 57.80 EUR/t to 143.79 EUR/t. In 2029, prices are likely to reach around 322.15 EUR/t (Figure 6).

The last figure (Figure 7) shows possible coal price movements forecast from 2008 to 2032. The upper and lower red line on the graph represent four standard deviations (or -/+ 2 St. dev.) or a 95% confidence interval, within which the movement of coal prices is likely to appear. The value

of two standard deviations increases over the years, from -/+ 30 EUR/t in 2007 to -/+60 EUR/t in 2021 and in 2032 to -/+ 100 EUR/t.[11]

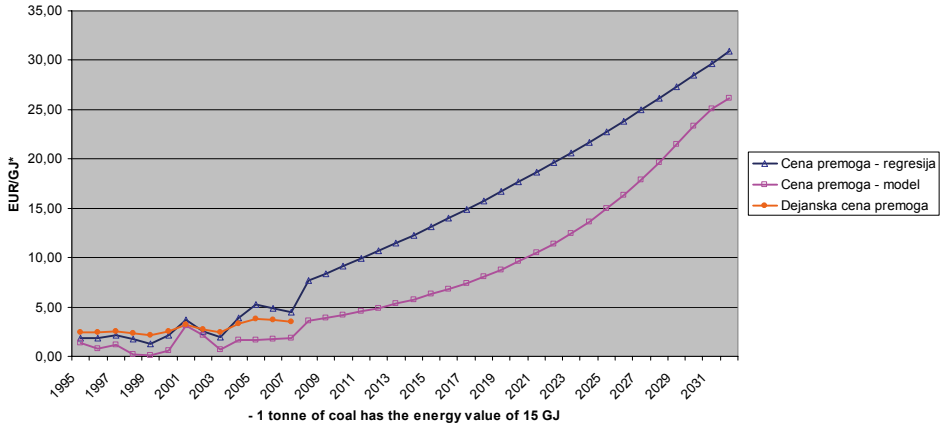

Figure 6: *Coal price movement forecast – annually.*

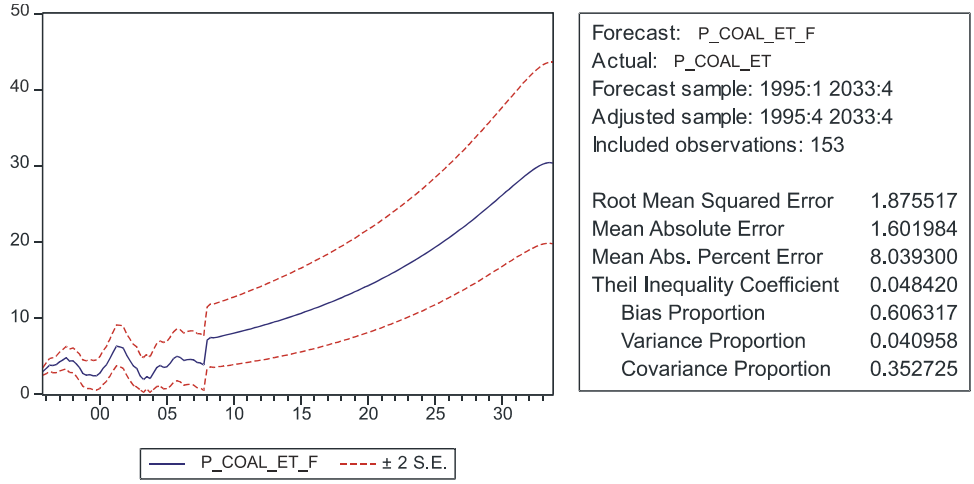

Figure 7: *Interval of confidence for forecasting coal prices.*

Note: Ordinate values are standardised and correspond to the ordinate values on Figure 7.

[11] The two assumptions of the forecast are that coal demand will grow mainly because of the growth of the Chinese and Indian economies. The EU Directive EC/2001/77 obliges EU member states to produce at least 33.6% of their electricity from renewable sources by 2010, which means (in accordance with the model given in Table 4) that increased environmental measures also increase the price of coal.

---

4 CONCLUSION

Coal – an important source for the production of primary energy – contributes one quarter of all primary energy production. According to some estimates, around 39-40% of global electricity requirements will be produced by coal until 2030. Thus, coal is likely to remain an important energy source in the future.

We estimated the influence of the consumption and price of other energy sources, environmental measures and the influence of electricity-market liberalization on coal price movements via the principal components method. The results show that if the price of other energy sources increases – specifically, if the price of crude oil increases by 3.695 EUR/barrel, the price of natural gas by 0.323 EUR/Mbtu and the price of uranium by 0.625 EUR/kg – the price of coal increases by 1.00 EUR/t. If the consumption of other energy sources increases so that the gross domestic electricity consumption increases by 48.583 kTOE, the gross domestic consumption of industrial waste by 41.121 kTOE, the gross domestic consumption of renewable sources by 771.065 kTOE, gross domestic consumption of crude oil by 489.402 kTOE, gross domestic consumption of natural gas by 2,225.218 kTOE and gross domestic consumption of nuclear energy by 635.998 kTOE, then the price of coal decreases by -1 EUR/t. If the energy industry contributes towards air pollution 3.678 kt CO, 2,566.487 kt CO_2 and 133.810 kt SO_x; and if the expenditures of environment protections in the whole EU25 industry sector increases by 298.206 million EUR, the share of consumption of renewable resources in primary energy production by 790.482 kTOE, taxes on environmental pollution by 171.456 million EUR and gross domestic consumption of renewable energy sources by 1,017.400 kTOE, then the price of coal will increase by 1 EUR/t. The increase of electricity prices by 1.799 EUR/MWh causes an increase in coal price of 1 EUR/t. The increase in the quotient of energy efficiency by 0.002 decreases coal prices by -1 EUR/t. If the dollar-euro exchange rate (EUR appreciation) increases by 0.032, the price of coal decreases by -1 EUR/t.

The prognosis for coal prices shows that it can be expected that the price of coal will increase from 57.80 EUR/t to 143.79 EUR/t in the period from 2009 to 2020.

References

[1] Baxter, M. J., Cool, H. E. M. and Heyworth, M. P. 1990. Principal component and correspondence analysis of compositional data: Some similarities. *Journal of Applied Statistics* 17: 229-235.

[2] Brečevič, D., Festić, M., Repina, S., Križanič, F., Cerjak Kovačec, A., Rojnik, E. and Bučar, A. 2008. Analiza in ocena cen energentov (Analysis and estimation of the prices of energy sources). Ljubljana: IREET and EIPF.

[3] Breusch, T. S. 1979. Testing for autocorrelation in dynamic linear models. *Australian Economic Papers* 17: 334-355.

[4] Catell, R. B. 1966. The scree test for the number of factors. *Multivariate Behavioral Research* 1: 245-276.

[5] Clean energy. 2008. About coal. [http://www.clean-energy.us/facts/coal.htm#world_resources], (6.5.2008).

[6] Dickey, A. D. and Fuller, A. W. 1979. Distribution of the estimators for autoregressive time series with unit root. *Journal of American Statistical Association* 74 (June): 427-431.

[7] EEX. European Energy Exchange. 2008. [http://www.eex.com/en], (9.6.2008)

---

[8] EIA. International Energy Outlook. Energy Information Administration. 2007. 2008. [http://www.eia.doe.gov/cneaf/coal/page/coalnews/coalmar.html, http://www.eia.doe.gov/emeu/iea/coal.html, www.iea.org/textbase/papers/2007/jr_price_interaction.pdf], (6.5.2008).

[9] Energy Security. 2008. Institute for the Analysis of Global Security. [http://www.iags.org/n0524044.htm], (9.4.2008).

[10] Energy. 2008. Fotovoltaica as the story of success. The green light for renewable sources directive. [www.energetika.net], (9.4.2008).

[11] Eurocoal. 2007, 2008. Euracoal's Market Report. [http://euracoal.be/], (19.5.2008).

[12] Eurocoal. 2007a. Euracoal's Market Report. [http://euracoal.be/newsite/Euracoal_Prognos_2007_engl.pdf 2007], (19.5.2008).

[13] Eurocoal. 2007b. The future role of coal in Europe. [http://euracoal.be/newsite/Euracoal_Prognos_2007_engl.pdf], (16.5.2008).

[14] Eurocoal. 2008a. [www.eia.doe.gov/cneaf/coal/page/coalnews/metcoalpricepost.xls], (6.5.2008).

[15] Eurocoal. 2008b. [http://euracoal.be/newsite/report.php], (19.5.2008).

[16] Eurostat concepts and definitions database. 2007. [http://circa.europa.eu/irc/dsis/coded/info/data/coded/en/Theme9.htm], (15.5.2008).

[17] Favero, C. A., Marcellino, M. and Neglia, F. 2005. Principal components at work: The empirical analysis of monetary policy with large datasets. *Journal of Applied Econometrics* 20 (5): 603-620.

[18] Fuentes, M. and Godoy, S. 2005. Sovereign spread in emerging markets: a principal component analysis. Banco Central de Chile Documentos de Trabajo. Central Bank of Chile, working paper, no. 333. [http://www.bcentral.cl/eng/studies/working-papers/pdf/dtbc333.pdf], (17.9.2008).

[19] Graffelman, J. and Aluja-Banet, T. 2003: Optimal representation of supplementary variables in biplots from principal component analysis and correspondence analysis. *Biometrical Journal* 45: 491-509.

[20] Harris, D. 1997. Principal components analysis of cointegrated time series. Econometric Theory 13: 539-557.

[21] Hartley, P., Medlock, K. B. and Rosthal, J. 2007. *The relationship between crude oil and natural gas.* Natural gas in North America: Markets and security. Rice University, Institute for public policy. [http://www.rice.edu/energy/publications/docs/natgas/ng_relationship-nov07.pdf], (10. 4. 2008)

[22] Kaciak, E. and Koczkodaj, W. 1989. A spreadsheet approach to principal components analysis. *Journal of Microcomputer Applications* 12 (1): 281-291. [http://www.stat.auckland.ac.nz/~iase/publications/18/BOOK1/A3-4.pdf], (18.6.2008).

[23] Kavalov, B. and Peteves, S. D. 2007. The future of coal. DG JRC, no. 22744. Institute for Energy. [http://ie.jrc.ec.europa.eu/publications/scientific_publications/2007/EUR22744EN.pdf], (14.5.2008).

[24] Kucewitz, W. 2007. Electricity prices in the fuel function. GeoInvestor. [http://goliath.ecnext.com/coms2/gi_0199-1511163/GeoInvestor-com-Florida-s-Looming.html], (19.5.2008).

---

[25] Lajevec, P., Bučar, A. and Brečevič, D. 2007. Oblikovanje nadzorovanih cen v energetiki (Formation of regulated prices in the field of energetics) Ljubljana: IREET. [http://www.ireet.com/slo/referati/modeli-oblikovanja-cen.pdf], (10. 4. 2008)
[26] Ramsey, J. B. 1969. Tests for specification errors in classical linear least squares regression analysis. *Journal of Royal Statistical Society* 31 (2, Series B): 350-371.
[27] Rao, C. R. 1964. The use and interpretation of principal component analysis in applied research. *The Indian Journal of Statistics* 26 (A): 329-358.
[28] Reinaud, J. 2007. CO2 Allowance & Electricity Price Interaction. Impact on industry's electricity purchasing strategies in Europe. IEA information paper. [http://www.iea.org/textbase/papers/2007/jr_price_interaction.pdf], (18.5.2008)
[29] Rovan, J. 2006. A multivariate analysis. Ljubljana. Economic Faculty.
[30] Sharma, G. Targetless scanner color calibration. *Journal of Imaging Science and Technology* 44 (4): 300-307.
[31] Statistical Review of World Energy. 2008. [http://www.bp.com/statisticalreview], (9.4.2008).
[32] Thursby, G. J. 1982. Misspecification, heteroscedasticity, and the Chow and Goldfeld-Quandt tests. *The Review of Economics and Statistics*, 64 (May): 314-321.
[33] WCI. World Coal Institute. 2004. Clean coal technology. Building a future through. Survey of energy resources. [http://www.worldcoal.org/], (19.5.2008).
[34] WCI. The World Coal Institute. 2007. 2008. The Coal Resource. [www.worldcoal.org/assets_cm/files/PDF/thecoalresource.pdf, http://www.worldcoal.org], (16.5.2008).
[35] WEC. World Energy Council. 2008. [http://www.worldenergy.org], (16. 5.2008).
[36] Wetzstein, E. M. and Green, R. D. 1978. Use of principal component attractiveness indexes in recreation demand functions. *Western Journal of Agricultural Economics* July: 11-22. [http://ageconsearch.umn.edu/bitstream/32405/1/03010011.pdf], (18.5.2008).

SOURCES:

1. EIPF and IREET. 2008. Internal data base.
2. EUROSTAT. 2008. URL [http://epp.eurostat.ec.europa.eu] (data on energy provisioning)
3. URL [www.agen-rs.si] (Slovenian regulator of energy market)
4. URL [http://www.ceer-eu.org/portal/page/ERGEG_HOME/ERGEG_DOCS/NATIONAL_REPORTS/2006] (National reports)
5. OECD. 2008. [http://lysander.sourceoecd.org/vl=1236089/cl=14/nw=1/rpsv/home.htm] (OECD data base on gas price and production in EU)
6. URL [http://search.atomz.com/search/?sp-a=sp10029401&sp-f=ISO-8859-1&sp-p=all&sp-q=gas+tranzit&spk=Web%20Content&sp-i=1]

SOFTWARE:

- Eviews 6.0
- SPSS 15.0
- Excel

LIST OF SYMBOLS:

Dlog	logarithm difference
b_x	coefficient of regression equations
FAC1_2, FAC2_2 in FAC3_2	main components of other energents consumption variables
FAC1_4	main component of energent price variables
FAC1_1, FAC2_1 in FAC3_1	main components of environmental measures variable
energy_effici	quotient between the available final consumption of energy and gross domestic consumption variable
a_ap_ei_co	Air pollution – energy industries CO
a_ap_ei_co2	Air pollution – energy industries CO_2
a_ap_ei_sox	Air pollution – energy industries SO_x
B_EPE_IND_TD	Environmental protection expenditure in EU – Manufacturing, total domains
P_OIL	The oil price - EUR/barrel
P_GAS	The gas price – EUR/Mbtu
P_COAL_ET	The coal price – average import price in EUR/t
P_URAN	The uranium price – EUR/kg
D_NRG_EFFICI_EFC	Supply, transformation, consumption – Energy available for final consumption
D_NRG_EFFICI_GIC	Supply, transformation, consumption – Gross inland consumption
E_NRG_SHARE_PP	Share of renewable energy – primary production
G_ELECTRICITY	The electricity prices in EUR for MWh – final industrial consumption
H_ETAXREVE	Environmental tax revenue – taxes on pollution in % of GDP
exch_r	dollar to euro exchange rate (expressed as a price for 1 EUR in dollars)
I_CON_ELECT	Gross consumption of electricity
J_CON_RENEWO02_IW	Consumption of renewable resources – industrial wastes (1000 toe)
J_CON_RENEW02_RE	Consumption of renewable resources – renewable energies (1000 toe)
L_CON_OIL	Crude oil and petroleum products consumption
M_CON_GAS	Gas consumption

N_CON_URAN Nuclear energy consumption

APPENDICES:

Table A: *Descriptive statistic of PCA analysis*

	N	Mean	Std. Deviation
a_ap_ei_co	52	563.3669	50.41557
a_ap_ei_co2	52	1454326.2571	35186.52533
a_ap_ei_sox	52	5714.8504	1834.53168
B_EPE_IND_TD	52	43607988.4725	4088405.84193
P_OIL	52	32.7829	19.62181
P_GAS	52	3.5029	1.71445
P_COAL_ET	52	42.9611	8.68069
P_URAN	52	6.2788	3.32317
D_NRG_EFFICI_EFC	52	1200364.1542	35658.88630
D_NRG_EFFICI_GIC	52	1686795.4615	57760.67369
E_NRG_SHARE_PP	52	898969.3088	10837.50864
G_ELECTRICITY	52	67.8031	6.05561
H_ETAXREVE	52	9284.7542	2364.36510
Euro/Dolar	52	1.1465	.15311
I_CON_ELECT	52	1109.4615	878.87505
J_CON_RENEWO02_IW	52	2879.8462	743.88111
J_CON_RENEW02_RE	52	99583.1550	13948.55899
L_CON_OIL	52	643870.3077	8853.27558
M_CON_GAS	52	384392.9235	40254.18904
N_CON_URAN	52	241590.3854	11505.19908
energy_effici	52	.7117	.00448
Valid N (listwise)	52		

Table B: *Histogram – normality test*

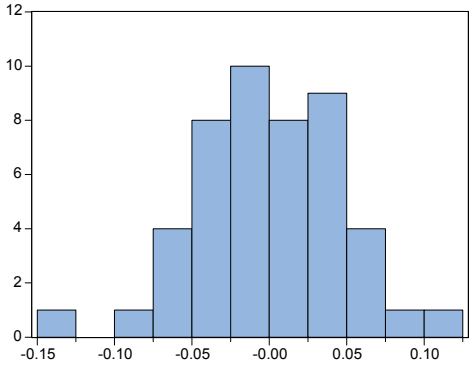

Series: Residuals	
Sample 1996:2 2007:4	
Observations 47	
Mean	0.000172
Median	-0.005412
Maximum	0.101374
Minimum	-0.133045
Std. Dev.	0.047710
Skewness	-0.174161
Kurtosis	3.219653
Jarque-Bera	0.332087
Probability	0.847009

Table C: *Autocorrelations*

Sample: 1996:2 2007:4, included observations: 47.

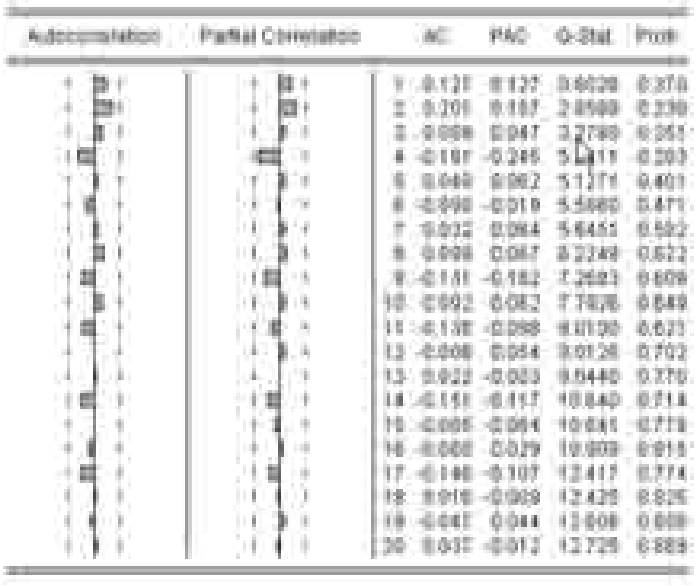

JET Volume 2 (2009), p.p. 41 - 54
Issue 2, June 2009

www.fe.uni-mb.si/JET

FLUID FLOW IN LONG RECTANGULAR MINICHANNELS AND MICROCHANNELS

TOK FLUIDA V DOLGIH IN PRAVOKOTNIH MINIKANALIH IN MIKROKANALIH

J. Avsec[✉], G. F. Naterer[1], A. Predin[2]

Keywords: fluid mechanics, microchannel flow, minichannel flow, micromechanics

Abstract

This article applies methods of statistical thermodynamics to analysis of fluid transport in minichannels and microchannels. The hydrodynamic equations are linearised and the governing equation of gas motion is reduced to the Stokes equation. The reduced mass flow through the microchannel is expressed in terms of the molecular mass, Boltzmann constant and rarefaction parameter. A key variable in estimating pressure differences within the microchannel is the apparent viscosity and thermal conductivity. In this regard, kinetic theory is applied with a Lenard–Jones potential to derive formulations of the microfluidic viscosity and thermal conductivity. The Chung-Lee-Starling model is applied to calculate viscosity and thermal conductivity. Numerical results are presented for property variations in fully developed flow through a long rectangular microchannel.

Povzetek

Predstavljen članek uporablja metode magneto-termodinamike za analizo toka fluida v mikrokanalih in minikanalih. Hidromehanske enačbe so linearizirane in enačba gibanja toka fluida je poenostavljena v Stokesovo enačbo. Ključna spremenljivka za izračun hitrostnih profilov

[✉] Assoc. Prof. Jurij Avsec, , Tel.: +386-7-620-2217, Fax: +386-2-620-2222, Mailing address: Hočevarjev trg 1, 8270 Krško, SLOVENIA, E-mail address: jurij.avsec@uni-mb.si
[1] Prof. dr. Greg F. Naterer, University of Ontario Institute of Technology, Oshawa, Ontario, Canada
[2] Prof. dr. Andrej Predin, University of Maribor, Faculty of Energy Technology, Hocevarjev trg 1, 8270 Krško, SLOVENIA

---

in eksergijskih izgub je poznavanje viskoznosti in toplotne prevodnosti fluida in elektromagnetnih lastnosti.

1 INTRODUCTION

Fluid flows through microchannels and capillaries of different forms arise in various emerging technologies, ranging from electronics cooling [1] to slip-flow control [2] and others [3]. In electronics cooling applications, previous analytical methods have been developed to predict Nusselt number variations in microchannels of various aspect ratios [1]. Previous studies give different views regarding the apparent viscosity in microchannel flows [4-6]. In certain cases, the apparent (required or measured) viscosity is reported to be much larger than the bulk viscosity at large distances away from the wall (Israelachvili [4]). However, in other studies conducted with flows in capillaries, the apparent and bulk viscosities are nearly equal (Anderson, Quinn [5]). Additional data for capillaries smaller than a micron in diameter was reported by Migun and Prokhorenko [6]. Pfahler et al. [7] give experimental data indicating that the apparent viscosity is smaller than the bulk viscosity of various liquids in microchannels (isopropyl alcohol, alcohol). The authors reported data for the liquid flow rate as a function of microchannel size, type of fluid and pressure drop across the microchannel.

A criterion involving the lateral wall influence on the microchannel flow rate was documented by Sharipov [8]. Rarefaction parameters at the ends of the microchannel are related to the mass flow rate. The kinetic equation model is applied over a range of Knudsen numbers and microchannel heights. The formulation extends from the hydrodynamic flow regime to the free molecular regime.

Experimental data regarding liquid flows in microchannels with hydraulic diameters ranging between 30 and 344 microns was reported by Xu et al. [9]. The range of Reynolds numbers was between 20 and 4,000. Their results indicate that flow characteristics agree with analogous behaviour predicted by the Navier-Stokes equations in the same range of Reynolds numbers. Heat transfer has been observed reducing frictional losses in microchannels, particularly at low Reynolds numbers [10]. At lower Reynolds numbers and temperatures, the fluid viscosity decreases and the wall friction becomes smaller. Such data was reported for three-dimensional flow variations of steady, laminar flow in a microchannel [10]. A relative temperature difference between the fluid and solid phases has been used to check the validity of local thermodynamic equilibrium assumptions in microchannels (Kim, Kim, Lee [11]).

When calculating the thermal conductivity and viscosity by methods of classical thermodynamics, curve fits of measured data are often used for interpolation over different ranges of temperature and pressure. Unlike these methods, statistical thermodynamics can provide a more rigorous and promising approach for microfluidic property evaluations, as it can accommodate intermolecular effects such as dipole moments. Theoretical developments of non-equilibrium transport properties, based on a velocity or temperature distribution function, have been documented by Ferziger and Kaper [12] and others [13, 14]. The velocity distribution function depends on the Knudsen number associated with the microchannel (Gad-el-Hak [3]). The distribution function can be expanded as a power series in terms of the Knudsen number, provided that the number is sufficiently small [3]. Translational, rotational, vibrational and electron excitation effects on property evaluation for pure refrigerants and other mixtures are

outlined by Avsec [15, 16]. This article extends these previous advances to predict variations of thermo-physical properties in microchannel flows.

2 FLUID FLOW IN MICROCHANNELS

2.1 Gas flow in microchannels

Gas motion through long microchannels can be predicted analytically with Shapirov's method [8]. In the fluid flow formulation, we will assume that the local pressure gradient is small, i.e.,

$$\nu = \frac{a}{p}\frac{dp}{dx}, \left|\nu\right| << 1 \tag{2.1}$$

This allows us to linearise the kinetic and hydrodynamic equations. We can express the reduced flow rate as follows,

$$\dot{Q} = -\frac{1}{abp\nu}\left(\frac{2kT}{m}\right)^{0.5}\dot{m} \tag{2.2}$$

where $\dot{m}$ is the mass flow rate through a cross-section of the channel, m is the molecular mass of the gas and k is the Boltzmann constant. It will be calculated as a function of the refraction parameter:

$$\delta = \frac{\sqrt{\pi}}{2}\frac{a}{\lambda} \tag{2.3}$$

where λ is the molecular mean-free path, which can be calculated via the pressure the shear viscosity, μ, as follows,

$$\lambda = \frac{\eta}{p}\left(\frac{\pi kT}{2m}\right)^{1/2} \tag{2.4}$$

where η is viscosity. In the hydrodynamic regime ($\delta \to \infty$), the gas flow is described by the following Stokes equation,

$$\eta\left(\frac{\partial^2 u'}{\partial y'^2}+\frac{\partial^2 u'}{\partial z'^2}\right)=\frac{dp}{dx'} \quad x=\frac{x'}{a},\ y=\frac{y'}{a},\ z=\frac{z'}{a},\ u=-\frac{1}{\nu}\left(\frac{m}{2kT}\right)^{1/2}u' \tag{2.5}$$

Equation (5) has the following solution:

$$u(y,z)=\frac{\delta}{2}\left(\frac{1}{4}-y^2-8\sum_{i=0}^{\infty}\frac{(-1)^i}{n^3}\frac{\cosh(nz)\cos(ny)}{\cosh\left(\frac{nb}{2a}\right)}\right),\quad n=\pi(2i+1) \tag{2.6}$$

The reduced flow rate can be expressed as:

$$Q_h = \frac{\delta}{6}\left(1 - 192\frac{a}{b}\sum_{i=0}^{\infty}\frac{1}{n^5}\tanh\left(\frac{nb}{2a}\right)\right) \tag{2.7}$$

Due to slip boundary conditions, Equation (2.7) is corrected through the following equation:

$$Q_s = Q_h + S$$

For small values of a/b, the slip term, S, can be approximated by the following formula:

$$S = \sigma_s\left(1 - 0.63\frac{a}{b}\right) \tag{2.8}$$

where σ_s is the slip coefficient.

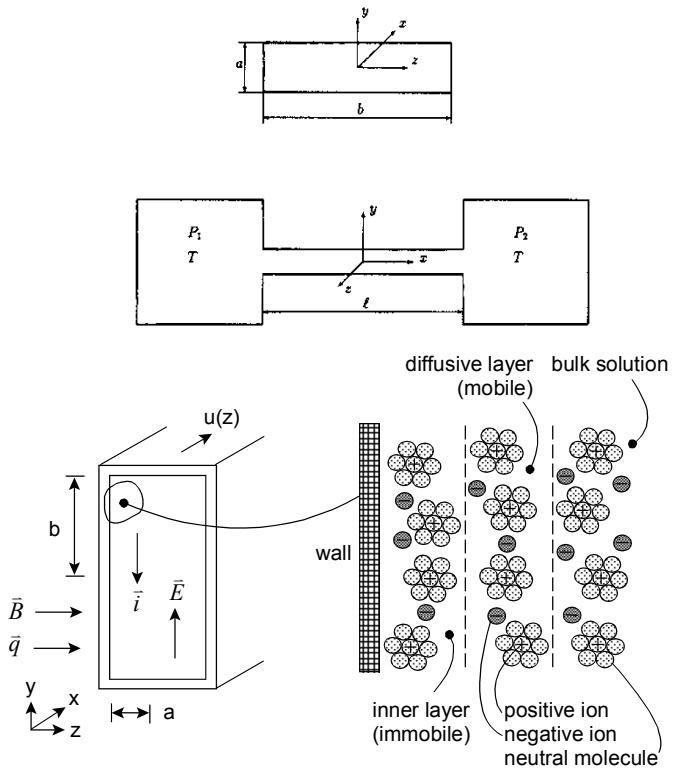

(a) (b)

Figure 1: *Schematic of (a) microchannel and (b) electric double layer.*

2.2 Influence of electro-thermomagnetic field

Electro-thermomagnetic effects on microfluidic transport have been reported previously in Refs. [17-21]. During electrokinetic flow in microchannels, the charged surface of a microchannel wall may attract ions of the opposite charge in the surrounding fluid. The resulting spatial gradient of ions near the wall leads to an Electric Double Layer (EDL). The EDL contains an immobile inner layer and mobile outer layer, which can be appreciably affected by an externally applied electric field. When we assume the fluid velocity, magnetic field and current density as orthogonal, we have the following reduced momentum equation:

$$0 = -\frac{dp}{dx} + \eta \frac{d^2u}{dz^2} + i_y B_z \tag{2.9}$$

The terms represent pressure, viscous and electromagnetic forces in the liquid. Using Ohm's Law to express the current density in terms of fluid velocity yields:

$$\eta \frac{d^2u}{dz^2} + \sigma_e B_z^2 u = \frac{dp}{dx}, \tag{2.10}$$

where σ_e and B_z refer to the electrical conductivity and magnetic field strength. For fully developed flow in a microchannel, the pressure gradient becomes constant and independent of the magnetic field strength. In terms of the Hartman number, M_H ($M_H = aB_z\sqrt{\sigma_e/\eta}$),

$$\eta \frac{d^2u}{dz^2} - \left(\frac{M_H{}^2 \eta}{a^2}\right) u = \frac{dp}{dx} \tag{2.11}$$

Applying the no-slip boundary conditions at z=a and z=-a, the analytical solution of Eq.(2.11) becomes:

$$u(z) = \frac{a^2\left(\frac{dp}{dx}\right)}{\eta M_H{}^2}\left(\frac{\cosh\left(\frac{M_H z}{a}\right)}{\cosh(M_H)} - 1\right) \tag{2.12}$$

The mean velocity within the microchannel becomes:

$$u_b = \frac{1}{2a}\int_{-a}^{a} u(z)dz = \frac{a^2\left(\frac{dp}{dx}\right)}{\eta M_H{}^2}\left(\frac{\sinh M_H}{M_H \cosh M_H} - 1\right) \tag{2.13}$$

When we non-dimensionless this result ($z^*=z/a$, $u^*=u/u_b$),

$$u^* = \frac{M_H \cosh M_H - M_H \cosh(M_H z^*)}{M_H \cosh M_H - \sinh M_H} \tag{2.14}$$

Without electromagnetic effects, Equation (11) transforms into the following expressions:

$$u(z) = \frac{a^2\left(-\frac{dp}{dx}\right)}{2\eta}\left(1-\left(\frac{z}{a}\right)^2\right) \tag{2.15}$$

$$u_b = \frac{1}{2a}\int_{-a}^{a} u(z)dz = \frac{a^2\left(-\frac{dp}{dx}\right)}{3\eta} \tag{2.16}$$

$$u^* = \frac{3}{2}\left(1-z^{*2}\right) \tag{2.17}$$

3 CONVECTIVE HEAT TRANSFER FORMULATION AND FORMULATION OF EXERGY LOSSES

For convective heat transfer within the microchannel, the transient, inertial and streamwise conduction terms can be neglected for small Reynolds numbers at steady states [17-18]. Then the reduced form of the energy equation becomes

$$\lambda\frac{d^2T}{dz^2} + \eta\left(\frac{du}{dz}\right)^2 + \frac{i_y^2}{\sigma_e} = 0 \tag{3.1}$$

Define the following non-dimensional temperature, ϑ, and electromagnetic coefficient, C

$$\theta\left(z^*\right) = \frac{\lambda(T-T_w)}{\eta u_b^{\,2}} \tag{3.2}$$

$$C = M_H\left(K-1\right)\cosh M_H - K\sinh M_H \tag{3.3}$$

where *K* represents a non-dimensional load factor (ratio of the applied electric field strength to the product of the mean velocity, u_b, and magnetic field strength).

In terms of the non-dimensional variables, the energy equation becomes

$$\frac{d^2\theta}{dz^{*2}} = -\left(\frac{du}{dz^*}\right)^2 - i_y^{*2} \tag{3.4}$$

$$i_y^* = -M_H(K-u^*) \tag{3.5}$$

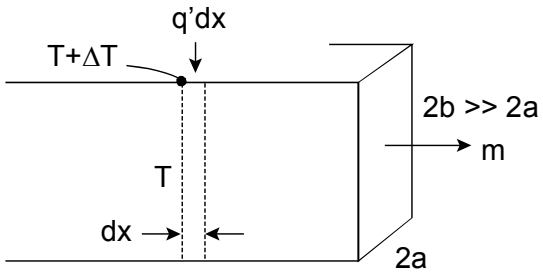

Figure 2: *Schematic of Heat and Mass Flow in a Microchannel*

The entropy production rate can be expressed as a sum of positive-definite terms corresponding to friction, thermal and electromagnetic irreversibilities, i.e.,

$$\dot{P}_s = \frac{\lambda \nabla T \nabla T}{T^2} + \frac{\eta \Phi}{T} + \frac{\sigma_e}{T}\left(\vec{E} + \vec{v} \times \vec{B}\right)\left(\vec{E} + \vec{v} \times \vec{B}\right) \tag{3.6}$$

In Equation (23), the terms on the right side represent a sum of squared terms, so the entropy production is positive, thereby complying with the Second Law of Thermodynamics. Based on the assumptions outlined previously in the fluid flow and heat transfer formulations, it can be shown that the reduced form of the entropy production equation can be written as

$$\dot{P}_s = \frac{\lambda}{T^2}\left(\frac{dT}{dZ}\right)^2 + \frac{\mu}{T}\left(\frac{du}{dz}\right)^2 + \frac{i_y^2}{\sigma_e T} \tag{3.7}$$

Define the following non-dimensional entropy production, $\dot{P}_s$, and wall temperature,

$$\dot{P}_s^* = \frac{\dot{P}_s}{\lambda / a^2},\ \theta_w = \frac{\lambda T_w}{\mu u_B^2} \tag{3.8}$$

Using these variables, the non-dimensional entropy production equation becomes

$$\dot{P}_s^* = \frac{\left(\frac{d\theta}{dz^*}\right)^2}{\left(\theta + \theta_W\right)^2} + \frac{\left(\frac{du}{dz^*}\right)^2}{\theta + \theta_W} + \frac{i_y{}^2}{\theta + \theta_W} \tag{3.9}$$

4 RESULTS AND DISCUSSION

The predicted results are illustrated in Figures 3-9. In Figure 3, the fluid viscosity decreases at lower temperatures, For fluid motion in microchannels, viscous dissipation in the streamwise direction generates internal energy. This creates a temperature rise and corresponding lower viscosity in Figure 3, which affects the resulting pressure loss and mass flow rate through the microchannel.

Viscous dissipation can have significance in microchannel flows, due to much higher surface to volume ratios than large-scale channels. Friction constant discrepancies with macro-scale theory may arise due to neglected temperature variations arising from viscous dissipation in microchannels. An average tube temperature may produce more reliable results than viscosity calculations based on the inlet temperature. However, the average fluid temperature is generally unknown before a solution is derived, as it involves the unknown velocity gradient through viscous dissipation in the thermal energy equation. As a result, analytical approximations of temperature changes based on expressions developed in Sections 2 and 3 can serve useful purposes.

Predicted velocity profiles without thermomagnetic effects are shown in Figure 4. As expected, parabolic profiles are obtained, similar to Poiseuille flow in tubes. Unlike the predicted trends in Figure 4, the near-wall velocity gradient increases at larger Hartmann numbers in Figure 5. The Hartmann number represents a ratio between electromagnetic and viscous forces on the fluid. When the relative magnitude of viscous forces become larger (at smaller Hartmann numbers), the wall friction increases. However, increasing electromagnetic forces (at larger Hartmann numbers) also lead to higher resistance of fluid motion. Thus, wall friction can be minimised by optimization of the Hartmann number and magnitude of the applied electromagnetic field within a microhannel.

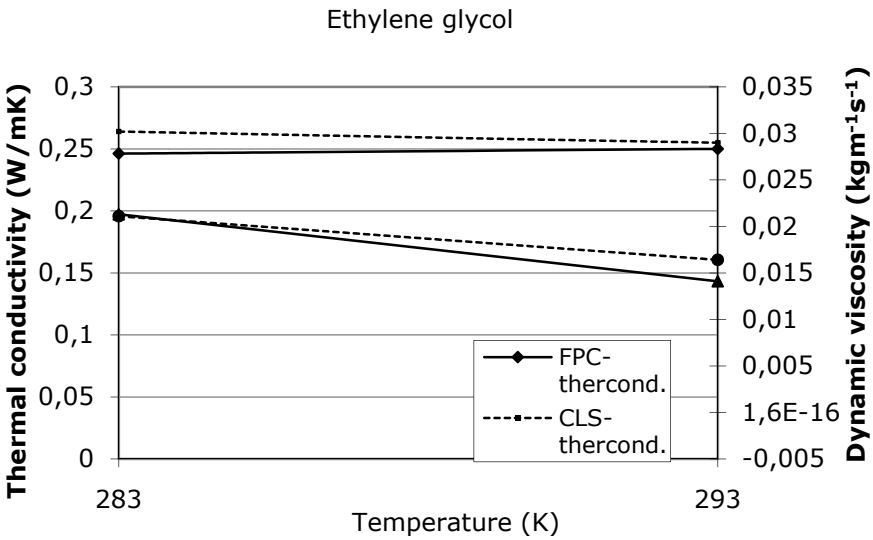

Figure 3: *Thermal conductivity and dynamic viscosity for liquid ethylene glycol.*

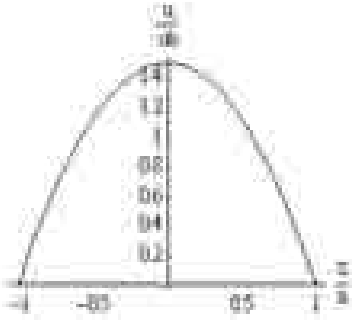

Figure 4: *Velocity profile without thermomagnetic effects.*

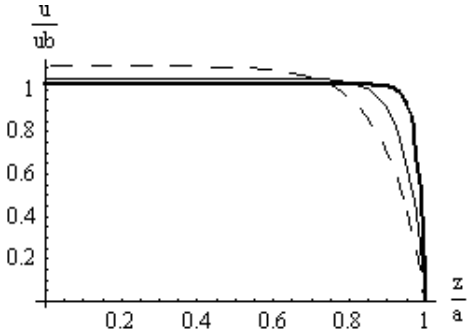

Figure 5: *Velocity (-- M_H=10, —— M_H=20, —— M_H=50).*

The predicted non-dimensional temperature is illustrated in Figure 6. Sensitivity studies were conducted to confirm that the temperature decreases at higher Hartmann numbers. The fluid resistance increases with larger electromagnetic fields, thereby reducing the mass flow rate and convective heat exchange between the walls and fluid. The trends of wall velocity gradient and mean velocity exhibit different trends, depending on whether the relative magnitude of electromagnetic forces exceeds viscous forces. For example, the wall velocity gradient decreased with *M* below approximately *M* = 2, while it increases thereafter. These trends have a direct impact on the temperature profile due to the convective heat exchange, which is affected by the velocity field, particularly close to the wall. Both friction and thermal irreversibilities are included in the entropy production results, which are illustrated in Figure 7.

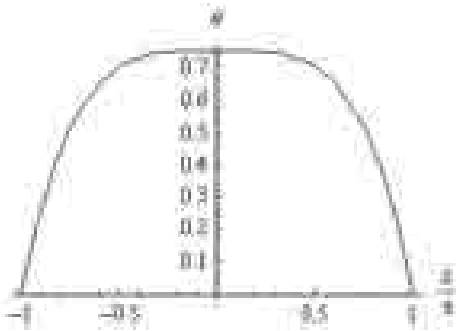

Figure 6: *Nondimensional temperature (without electromagnetic effects).*

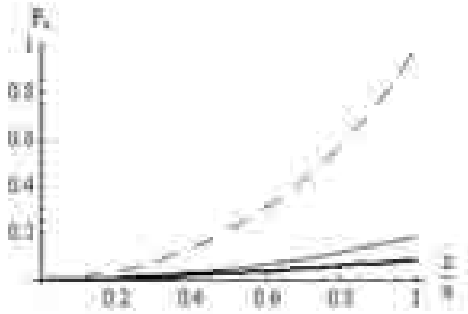

Figure 7: *Non-dimensional entropy production (-- $\vartheta_w = 10$, —— $\vartheta_w = 20$, —— $\vartheta_w = 50$).*

Additional results of non-dimensional temperature and entropy production are shown in Figure 8. Further sensitivity studies showed that the temperature decreases at lower Hartmann numbers. The mean velocity increases with smaller electromagnetic resistance of the fluid motion, which increases the denominator in the non-dimensional temperature. Furthermore, the near-wall temperature gradient increases at larger Hartmann numbers. This suggests that a larger electromagnetic field tends to increase the rate of convective heat transfer from the wall. The electromagnetic field generates Ohmic heating within the microchannel, which increases the thermodynamic irreversibilities and dissipation of kinetic energy to thermal energy within the fluid. In addition to controlling mass transport through a microchannel, it appears that the applied electric field can be manipulated for purposes of thermal control of fluid temperature within a microchannel.

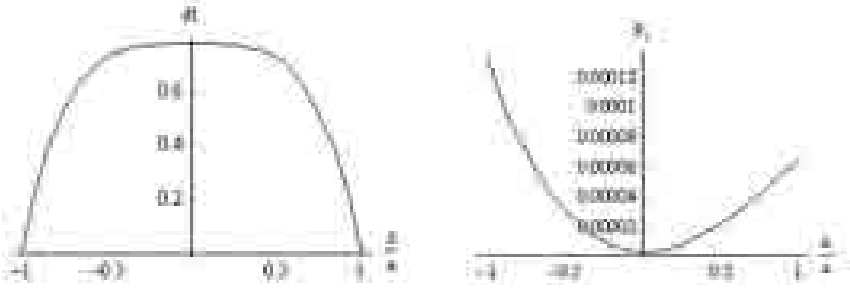

Figure 8: *Non-dimensional temperature and entropy production fields (constant wall temperature).*

5 CONCLUSIONS

This paper develops a formulation of fluid motion, thermophysical properties and entropy production in microchannel flows. Friction, thermal and electromagnetic irreversibilities have significance in energy efficiency of microfluidic systems. For example, additional input power is needed to overcome these irreversibilities to deliver specified rates of mass flow and heat exchange within a microchannel. The results indicate that entropy and the Second Law have significance in electrokinetic liquid transport through microchannels.

References

[1] Zhao, C. Y., Lu, T. J., "Analysis of Microchannel Heat Sinks for Electronics Cooling", International Journal of Heat and Mass Transfer, vol. 45, no. 24, pp. 4857-4869, 2002

[2] Naterer, G. F., ``Adaptive Surface Micro-Profiling for Microfluidic Energy Conversion'' (to appear), AIAA Journal of Thermophysics and Heat Transfer, vol. 18, no. 3, 2004

[3] Gad-el-Hak, M., ``The Fluid Mechanics of Microdevices – The Freeman Scholar Lecture'', ASME Journal of Fluids Engineering, vol. 121, pp. 5-33, March 1999

[4] Israelachvili, J. N., ``Measurement of the Viscosity of Liquids in Very Thin Films'', Journal of Colloid and Interface Science, vol. 11, no. 1, pp. 263-271, 1986

[5] Anderson, J. L., Quinn, J. A., ``Ionic Mobility in Microcapillaries'', Faraday Transactions I, vol. 68, pp. 744-748, 1972

[6] Migun, N. P., Prokhorenko, P. P., ``Measurement of the Viscosity of Polar Liquids in Microcapillaries'', Colloid Journal of the USSR, vol. 49, no. 5, pp. 894-897, 1987

[7] Pfahler, J., Harley, J., Bau, H., Zemel, J. N., ``Gas and Liquid Flow in Small Channels'', Symposium on Microelectromechanical Sensors, Actuators and Systems, vol. 32, pp. 49-60, 1991

[8] Sharipov, F., "Rarefied Gas Flow through a Long Rectangular Channel", Journal of Vacuum Science and Technology A, vol. 17, no. 5, pp. 3062-3066, 1999

[9] Xu, B., Ooti K. T., Wong N. T., Choi W. K., "Experimental Investigation of Flow Friction for Liquid Flow in Microchannels", International Communications in Heat and Mass Transfer, vol. 27, no. 8, pp. 1165-1176, 2000

[10] Toh, K. C., Chen X. Y., Chai, J. C., "Numerical Computation of Fluid Flow and Heat Transfer in Microchannels", International Journal of Heat and Mass Transfer, vol. 45, no. 26, pp. 5133-5141, 2002

[11] Kim, S. J., Kim, D., Lee, D. Y., "On the Local Thermal Equilibrium in Microchannel Heat Sinks", International Journal of Heat and Mass Transfer, vol. 43, no. 10, pp. 1735-1748, 2000

[12] Ferziger, J., Kaper, H. G., Mathematical Theory of Transport Processes in Gases, North-Holland Publishing Company, London, 1972

[13] Kihara, T., Intermolecular Forces, University of Tokyo, John Wiley & Sons, New York, 1976

[14] Chapman, S., Cowling, T.G., The Mathematical Theory of Non-Uniform Gases, Third Edition, Cambridge, University Press, 1970

[15] Avsec, J., ``Calculation of Transport Coefficients of R-32 and R-125 with the Methods of Statistical Thermodynamics and Kinetic Theories of Gas'', Archives of Thermodynamics, vol. 24, no. 3, pp. 69-82, 2003

[16] Avsec, J., ``Calculation of Equilibrium and Nonequilibrium Thermophysical Properties by Means of Statistical Mechanics'', Journal of Technical Physics, vol. 44, pp. 1-17, 2003.

[17] Naterer, G.F., Effects of Thermomagnetic Irreversibilities on Microfluidic Transport, AIAA 2005-5327, 38th AIAA Thermophysics Conference, June 6-9 2005, Toronto, Canada.

[18] Naterer, G.F., Adeyinka O.B., Microfluidic exergy loss in a non-polarized thermomagnetic field, International Journal of Heat and Mass transfer, Vol. 48 (2005), pp. 3945-3956.

[19] Horiuchi, K., Dutta, P., Joule Heating Effects in Electro-osmotically Driven Microchannel Flows, International Journal of Heat and Mass Transfer, Vol. 47 (2004), pp.:3085-3095.

[20] Hetsroni, G., Mosyak, A., Pogrbnyak, E., Yarin, L.P., Fluid Flow in micro-channels, International Journal of Heat and Mass Transfer, Vol. 48 (2005), pp.:1982-1998.

[21] White,F.M., Fluid Mechanics, McGraw-Hill, Fifth Edition, 2003, International Edition.

Nomenclature

(Symbols)	(Symbol meaning)
a	dimension of microchannel
b	dimension of microchannel
B	magnetic field strength
c_p	specific heat capacity at constant pressure
CLS	Chung-Lee-Starling
F	number of degrees of freedom
i	current density
k	Boltzmann constant
L	length of microchannel
LJ	Lennard-Jones
M	molecular mass
M_H	Hartmann number
$\dot{m}$	mass flow rate
N	number of molecules in system
P	Pressure
$\dot{P}_s$	entropy production rate
Q	heat flux
R_m	universal gas constant
t	Time
T	Temperature
T^*	reduced temperature
T_c	critical temperature
V	Volume
V_c	critical volume
Z_{coll}	collision number
x,y,z	Cartesian coordinates
β	diffusion term
ε	Lennard-Jones parameter
η	dynamic viscosity
λ	thermal conductivity
μ	reduced dipole moment
n	local pressure gradient

κ	correction factor for hydrogen bonding effect
ρ	Density
σ	Lennard-Jones parameter
σ_e	electrical conductivity
σ_s	slip coefficient
ψ	influence of internal degree of freedom
ω	acentric factor
Ω	collision integral
Ω^*	reduced collision integral

JET Volume 2 (2009), p.p. 55 - 64

Issue 2, June 2009

www.fe.uni-mb.si/JET

DETERMINING OPTIMAL SIZE, POSITION AND COVERING MATERIAL FOR A BUSHING SHIELD

DOLOČITEV OPTIMALNE VELIKOSTI, POZICIJE IN MATERIALA OBLOGE ZA ZASLON SKOZNJIKA

A. Glotić ℜ, P. Kitak, J. Pihler, I. Tičar

Keywords: differential evolution, optimization, electrical field, insulating elements, shield

Abstract

This paper deals with the design optimization of insulating elements - bushings. The principle of the shield size and its position as well as the insulating material determination, based on an optimization process is presented on the example of a bushing. The aim of the optimization was to achieve lowest electrical field strength values around a bushing and the lowest ratio of the electrical field strength values at the border of two different dielectric materials; the bushings body and the dielectric layer that covers a shield. High electrical field strength values are one among factors, which can dramatically decrease the insulators' operational reliability; therefore the optimal design of a bushing with lowest electrical field strength values is desirable. An optimization procedure was carried out using Differential Evolution (DE) Algorithm combined with the solver of the software tool EleFAnT for solving a parametrically-written model of a bushing. EleFAnT is based on finite element method (FEM) with a pre-processor that was made in the MATLAB software tool.

ℜ Corresponding author: Adnan Glotić, Tel.: +386 2 220 7175, Fax: +386 2 252 5481, Mailing address: University of Maribor, Faculty of electrical engineering and computer science, Smetanova ulica 17, 2000 Maribor, Slovenia. E-mail address: adnan.glotic@uni-mb.si

---

Povzetek

Članek obravnava optimizacijo modelov izolacijskih elementov oz. skoznjikov. Princip določitve velikosti, pozicije ter materiala obloge zaslona, ki temelji na optimizacijskem postopku, je prikazan na primeru skoznjika. Namen optimizacije je doseganje najnižjih vrednosti električnega polja okoli skoznjika ter najnižjega razmerja električnih poljskih jakosti na meji med dvema materialoma, in sicer med telesom skoznjika in oblogo zaslona. Visoke vrednosti polja lahko močno znižajo zanesljivost delovanja izolatorjev, zato je optimirani model skoznjika, ki ima najnižje možne vrednosti električnega polja zaželen. Optimizacijski postopek je izveden z uporabo algoritma diferenčne evolucije (DE) v kombinaciji s solverjem programskega orodja EleFAnT, ki se uporablja za reševanje parametrično zapisanega modela skoznjika. EleFAnT temelji na metodi končnih elementov, predprocesor, ki omogoča parametrični zapis modela pa je realiziran v programskem orodju MATLAB.

1 INTRODUCTION

The principal function of insulators is the electrical insulation of the conductive parts from the grounded parts, and the mechanical fixing of equipment and conductors that have different potentials [1]. Insulators are used in practically all parts of electric power system and, consequentially, they have a great impact on its operational reliability. They have also gained additional importance with the introduction of an open electrical energy market, which has sharpened circumstances at the areas of interruptions and disturbances in the electrical energy supply. Because of this, it is important that these elements are designed with care and are reliable during operation.

The operational reliability of insulators depends beside other factors, also on electrical field strength values, so one of the most important criterions for insulator design is correct dimensioning with regard to the electrical field strength [2]. Electrical field calculations and analyses for this purpose were made using the software tool EleFAnT (Electromagnetic Field Analysis Tools) [3]. The current practice in designing of insulating elements is the use of optimization algorithms. The optimization procedure in this paper was carried out by using an optimization algorithm, which is in the class of Evolutionary Algorithms.

2 MODELING AND OPTIMIZATION OF INSULATING ELEMENTS

2.1 Bushings

Bushings are elements of switchgear devices. They are used for guiding the conductors, which have a certain electrical potential, through the metal walls. Essentially, they consist of an insulating body often made from epoxy resin (dielectric constant $\varepsilon_r = 4.3$), which is poured around a metal cylinder. The most important criterion for bushing designing is correct dimensioning with regard to the electrical field strength. Its values in the observed area of the bushing must be lower than the permissible value for any particular insulating material, i.e. dielectric. Field shaping is required in cases where electrical field strength exceeds the insulator's dielectric strength in a certain part of the observed area. The main measure for electrical field shaping is the insertion of the so-called shield into the insulating body of the bushing.

The shield is a thin metal mesh or sheet, which is poured into the insulating body. This represents the equi-potential plane that shapes the electrical field. The results of field shaping are greater electrical field strengths inside the insulating body, which have a great dielectric strength (30 MV/m). Thus, the surrounding air, whose dielectric strength is inappropriately smaller (3 MV/m), is discharged.

Figure 1: *Picture of different bushings.*

Bushing bodies are usually made of a single insulating material and when describing the insulators structure we often forget on presence of one more insulating material - the surrounding air. The dielectric constant of air ($\varepsilon_r = 1$) is much lower than the dielectric constant of a epoxy resin, which can be, in some cases, the main reason for its high electric stress appearance. In cases where the electric field strength is normal to the bounding surface of two dielectrics, the electric stress distribution is in inverse ratio to their dielectric constants. In addition, the electrical breakdown strength of air, which is 3 MV/m, is 10 times lower than the electrical breakdown of the bushing's body. These facts lead to the conclusion that there is a great possibility for the highest values of electric field to occur within the air. These higher values are, according to results, located near the boundary surfaces of dielectrics, in our case on insulator's outer surface. These locations are known to be weak points in insulating systems, where high electric field values can give rise to corona and discharge activity. This can degrade the performance of body's material, causing permanent damage to the body and the breakdown of the insulators is a distinct possibility. Because of this, it is favorable to reduce the electric field in high stress areas. This can be achieved by insertion of a metal shield and appropriate selection of covering material. The shield’s size and position, as well as the appropriate selection of covering material can be determined by employing the optimization algorithm into the determination process. The final result is greater operational reliability of the insulator alone as well as greater operational reliability of the whole system of which the insulator is part off.

According to Figure 1 it can be concluded that the object in our study practically enables 2D numerical analysis due to the rotational symmetry. Electric field calculation requires the building of a 2D model of the bushing. In addition to geometry, the building of a model requires setting-up the model's attributes, which means that dielectric constants of various bushing

components have to be defined, as well as the boundary conditions. The discussed bushing belongs to 24 kV equipment and, according to the adequate standards calculations of electrical field distribution, were made at a test voltage of 125 kV.

After setting up the boundary conditions, discretization followed in which the mesh generator partitioned the modeling region into a net of finite elements (Figure 2a). The last step after discretization of the modeling region is the calculation of electric field distribution for initial model geometry (Figure 2b).

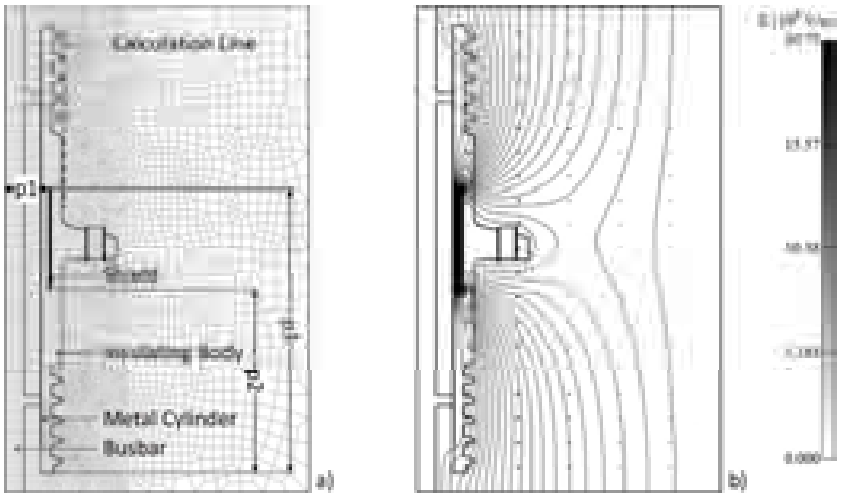

Figure 2: a) *Discretized model of bushing and the optimization parameters* ***b)*** *Electrical field plot*

2.2 Modeling algorithm

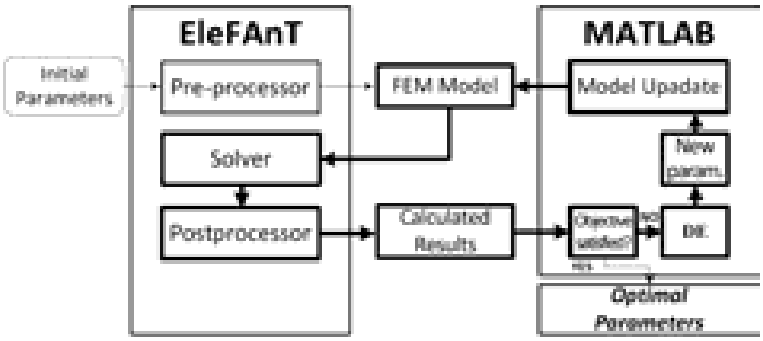

Figure 3: *Schematic presentation of modeling algorithm.*

In the past, the modeling of insulating elements had the following procedure: the first phase was shape and material selection for those parts that compose an insulator. The selection was mainly based on previous experiences. After this phase, the electric field computation followed. This calculation was employed for verifying that electric field values were kept below the values of dielectric breakdown strength with all critical parts. The design geometry modifications and necessary computations were made until the requirements regarding highest values of electric

field strength were met. However, this procedure is very time consuming, especially the necessary preparation of new models for each individual computation. To overcome this problem, the use of an optimization algorithm in modeling process is necessary.

The modeling algorithm (Figure 3) consists of four basic modules: a parametrically-written model, automatic mesh generator, solver of the software tool EleFAnT and an optimization algorithm. The object on which we have applied a modeling algorithm was a FEM model of a bushing. A parametrical description of a model is required for the optimization purposes, and it has a several advantages; for example, the possibility of a quick and simple geometry modification, which enables the analyses of different solutions within short period of time. The second advantage worth pursing is the possibility of employing different optimization algorithms. In our case, the optimization algorithm employed to indentify optimal parameter values for the most favorable electric field distribution is Differential Evolution (DE) algorithm.

The objective of the optimization algorithm was to reduce electric field strength in the most critical parts of the insulating element, because these values have a great impact on element's operational reliability. The most used algorithms in design optimizations of such equipment are evolutionary algorithms. These imitate the principle of natural evolution, which is the main reason for the use of terminology that is related to this field of science. Thus, the evolutionary algorithms operate over individuals (candidates for solution) or populations (set of individuals) by means of selection and operators like mutation and crossover, which produce better solutions from generation to generation.

2.3 Differential evolution

DE [4] is a simple evolutionary algorithm in which individuals or solution candidates are written in vector form. This form is needed for the ability to sum them and multiply with the scalar as the procedure for new candidates' generation (creation) demands. DE is a so-called steady-state optimization algorithm in which new candidates do not compose the entire new population, but they are simply added into existing one. This method accelerates the convergence of the algorithm because the currently calculated quality individuals are immediately used for the new candidates' generation. Besides the good convergence properties of DE, its algorithm is simple to understand and to implement. DE is also particularly easy to work with, having only few control variables, which remain fixed throughout the entire optimization procedure. DE utilities *NP D*-dimensional parameter vectors that have the form

$$\boldsymbol{x}_{i,G} = \left[x_{1,i,G}, x_{2,i,G}, ..., x_{D,i,G} \right];\ i = 1, ..., NP, \tag{2.1}$$

where *G* is the generation number and *NP* number of population.

The initial population is chosen randomly from the parameter space, which is defined with lower and upper bounds for each parameter $x_j^L \le x_{j,i,1} \le x_j^U$. Initial parameter values should cover the intervals $\left[x_j^L, x_j^U \right]$ uniformly. Each of the *NP* parameter vectors undergoes mutation, recombination and selection. Mutation expands the search space. For each parameter vector, $\boldsymbol{x}_{i,G}$ a perturbed vector $\boldsymbol{v}_{i,G+1}$ is generated according to

$$\boldsymbol{v}_{i,G+1} = \boldsymbol{x}_{r1,G} + F\left(\boldsymbol{x}_{r2,G} - \boldsymbol{x}_{r3,G} \right), \tag{2.2}$$

---

with $r_1, r_2, r_3 \in [1, NP]$, integer and mutually different, and $F > 0$.

The vectors $\boldsymbol{x}_{r1,G}$, $\boldsymbol{x}_{r2,G}$ and $\boldsymbol{x}_{r3,G}$ are randomly selected from the current population such that the indices *i*, r_1, r_2 and r_3 are distinct. *F* is a real and constant factor $\in [0,2]$, called crossover factor which controls the amplification of the differential variation $(\boldsymbol{x}_{r2,G} - \boldsymbol{x}_{r3,G})$. The vector $\boldsymbol{x}_{r1,G}$ which is perturbed to yield $\boldsymbol{v}_{i,G+1}$ has no relation to $\boldsymbol{x}_{i,G}$ but is a randomly chosen population member. In order to increase the diversity of the new parameter vector, crossover is introduced. Crossover incorporates successful solutions from the previous generation. The trial vector $\boldsymbol{u}_{i,G+1}$ is developed from the elements of the target vector $\boldsymbol{x}_{i,G}$ and the elements of the perturbed vector $\boldsymbol{v}_{i,G+1}$. Elements of the perturbed vector enter the trial vector with a crossover probability *CR*

$$u_{j,i,G+1} = \begin{cases} v_{j,i,G+1} \text{ if } \text{rand}_{j,i}[0,1] \le CR \text{ or } j = I_{rand} \\ x_{j,i,G} \text{ if } \text{rand}_{j,i}[0,1] > CR \text{ or } j \ne I_{rand} \end{cases}, \tag{2.3}$$

where $\text{rand}_{i,j} \in [0,1]$ and I_{rand} is a random integer from $[1,2,...,D]$. I_{rand} ensures that a trial vector $\boldsymbol{u}_{i,G+1}$ cannot be a duplicate of a target vector $\boldsymbol{x}_{i,G}$. To decide whether or not it should become a member of generation *G*+1, the new vector $\boldsymbol{u}_{i,G+1}$ is compared with the target vector $\boldsymbol{x}_{i,G}$ and the one with lowest function value is admitted to the next generation

$$\boldsymbol{x}_{i,G+1} = \begin{cases} \boldsymbol{u}_{i,G+1} \text{ if } f(\boldsymbol{u}_{i,G+1}) < f(\boldsymbol{x}_{i,G}) \\ \boldsymbol{x}_{i,G} \text{ otherwise} \end{cases}, \tag{2.4}$$

where $i = 1,2,...,NP$. Mutation, recombination and selection continue until stopping criterion.

2.4 Objective function

The optimization algorithm was employed for determination of the optimization parameters that provide the lowest possible electrical field strength values around a bushing. During the investigation on bushing behavior, when applying material properties changes, we have discovered that a thin layer of dielectric material around the shield (in our case 1 mm thin lining) has an impact on electrical field strength values in the surrounding air around a bushing. Figure 4 shows a plot of electrical field strength values in the external air around a bushing for three different examples (calculated on calculation line shown in Figure 2a). All three calculations were performed at withstand voltage of 125 kV. In case of bushing without a shield, its electrical field strength values exceed dielectric strength of the surrounding air (3 MV/m). In case of a bushing with a shield, the field forms so that its highest value is lower than the permissible one. Coverage of the same shield with a 1 mm thin layer of a dielectric material (ε_r = 9) that has a greater dielectric constant than insulators body (ε_r = 4.3), causes a small enlargement of the electrical field strength values in the external air. It can be assumed now that a selection of correct material for shields covering will give us the ability to lower electrical field strength values under the minimum that can be achieved with the optimal shield size and position alone. In contrast, the field distribution in the area around the shield is such that practically only the normal component of electrical field exists. This means that electrical field

strength values at the border of two dielectric materials are in the reverse ratio of the material's dielectric constant. This statement leads us to the conclusion that the greater the difference in material dielectric constants is, the greater is the change in electrical field strength values when crossing the border of the discussed materials. This difference should also be low as much as possible, because the greater the difference, the greater the negative impact is on the material's ageing and its properties.

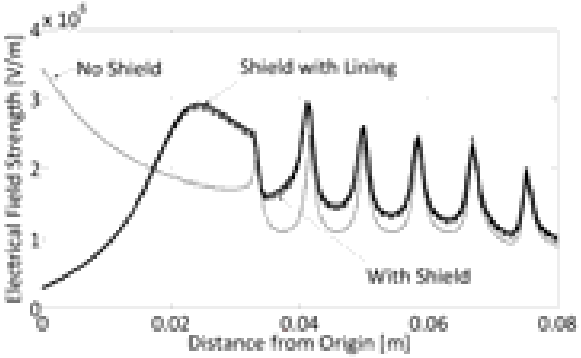

Figure 4: *Electrical field strength observed on calculation line (presented in Figure 2).*

Since the goal of the optimization, in our case, is to achieve the lowest electrical field strength values in the air around the bushing with regards to the difference of the electrical field strength values at the border of two materials, it is necessary to merge these two different objectives into single one. The first objective is the lowest value of electrical field strength in the surrounding air of a bushing; the second one is a ratio of electrical field strength values at the border of two dielectric materials, which should be as much as possible near 1. It can be seen that we are dealing with two different objectives, which have to be treated simultaneously (multi-objective optimization). Also, these two objectives are in conflict with each other, which means that improvement in one objective, worsens the other one. In our case, we are dealing with two different quantities, so if we want to merge these two objectives, the objective function values must be relative. Using membership functions, it is possible to quantify in relative values how much the particular set of parameters satisfies the requirements of each objective. In general, two different types of objectives can be distinguished: *best fit* objectives and *minimum* objectives. In our case, the best fit objective $f_r(\boldsymbol{x})$, in which the function value should reach a reference quantity as close as possible to 1, is used for the electrical field strength ratio, while the minimum objective is $f_E(\boldsymbol{x})$, in which the function value (electrical field strength value around a bushing) should become as small as possible.

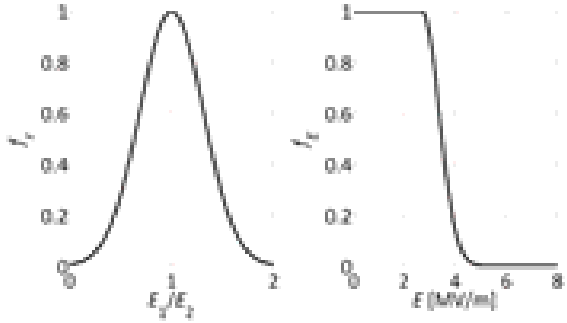

Figure 5: *Best fit (left) and minimum objective function (right).*

Both objective functions are analytically given by bell shaped fuzzy sets (Figure 5) and merged into a unified objective function $f(\boldsymbol{x})$ by weighting the objectives. With this technique, we are attempting to optimize a weighted sum of both objectives

$$f(\boldsymbol{x}) = w_E f_E(\boldsymbol{x}) + w_r f_r(\boldsymbol{x}), \tag{2.5}$$

where w_E and w_r are weights of individual quantities.

The main drawback of this technique lies in the choice of the weights that have the two-fold purpose of normalizing the objectives in order to obtain a balanced sum and of implementing a hierarchy of the objectives giving priority to one instead of other. In the preparation of the objective function, an electrical field strength values ratio of 1 was defined as the *best fit* value for $f_r(\boldsymbol{x})$, and an electrical field strength of 2.7 MV/m as the *minimum* value for $f_E(\boldsymbol{x})$. Since the greater emphasis in the optimization was given to electrical field strength, the weighting factors in equation (2.5) were set at $w_r = 0.35$ and $w_E = 0.65$.

3 RESULTS

An initial model of a bushing with a parametrically written geometry and material properties was entirely submitted to the optimization algorithm. Parameter boundaries are presented in Table 1.

The primary objective of the optimization was to achieve a favorable distribution of electrical field around a bushing and the secondary objective was to find a good selection of a dielectric material to cover the shield. Good material selection enables lower electrical field strength values around the bushing, but the change of electrical field when crossing a border of two dielectric materials should be low as much possible.

Table 1: *Values of optimization parameters*

Parameter	p_1 (mm)	p_2 (mm)	p_3 (mm)	p_4
Lower bound	45	118.0	276.0	2.00
Upper bound	55	194.0	352.0	10.00
Optimal value	45	157.2	320.8	3.71

The results of the optimization in Table 1 are values of parameters that determine shield size and position as well as the dielectric constant of the shields covering material (parameter p_4). The optimization results were gained by following DE control parameters: number of population $NP = 20$, crossover probability $CR = 0.8$, and scaling factor $F = 0.5$.

The convergence course of the optimization is shown in Figure 6. The objective function value in each generation was subtracted from value 1 in order to display “minimization” of the objective function, although the value 1 represents the best satisfaction of the objective function.

During the optimization process, the uniformed objective function $f(\boldsymbol{x})$ had been evaluated for each of the 20 individuals in every single population (generation). The minimum of the objective function was approached after 127 generations and 2,540 function evaluations (iterations of the FEM code). The parameter trajectories of the best individual in every generation are displayed in Figure 7.

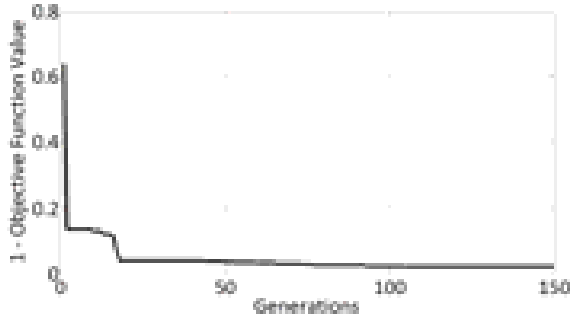

Figure 6: *Convergence course of the optimization.*

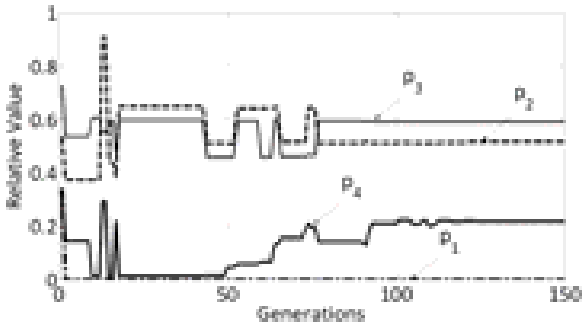

Figure 7: *Parameters trajectories of best individual in every single population (generation).*

Parameters in Figure 7 are presented in relative form for easier reading. The parameter p_4 stands out with its changes until the 120th generation, while other parameters had mostly settled before the 90th generation. This parameter presents the dielectric constant of a shield covering whose changes resulted the variations in ratio of electric field strength values and, consequently, the variations in $f_E(\boldsymbol{x})$ function values. Since two different objectives had been merged into one objective, the mutual impact was expected.

Figure 8a shows a premature convergence in the electrical field strength value towards the minimum value. After about 500 function evaluations, the minimum value was almost reached, but change in values continued for about another 2,000 function evaluations. The reason for this was change of the convergence course of electrical field strength values ratio. As can be seen from Figure 8b, the algorithm was misleading. Figure 8d presents the distribution of the ratio values. It is clearly seen that the parameter p_4 started towards one value and later it changed the course toward a different value. The first course of this parameter was toward the lower bound of the parameter p_4 ($\varepsilon_r = 2$), which had the greatest impact on lowering the electrical field strength values around the bushing. There are around 300 scores of equal values (ratio = 0.466). The best value for electrical field strength regarding uniform objective function was 2.73 MV/m (950 equal scores). When parameter p_4 was on its lower bound, electrical field strength values reached value of 2.71 MV/m. The number of scores in Figure 8c that corresponds to value of 2.71 MV/m is the same as previously mentioned (300). Although the lowest value of electrical field strength is 2.71 MV/m, this is not a final result because we did not give a total priority to a minimum of objective function $f_E(\boldsymbol{x})$. The objective was to find a compromise between lowest electrical field strength values around the bushing and the lowest electrical field strength values ratio on the boundary of two different dielectric materials.

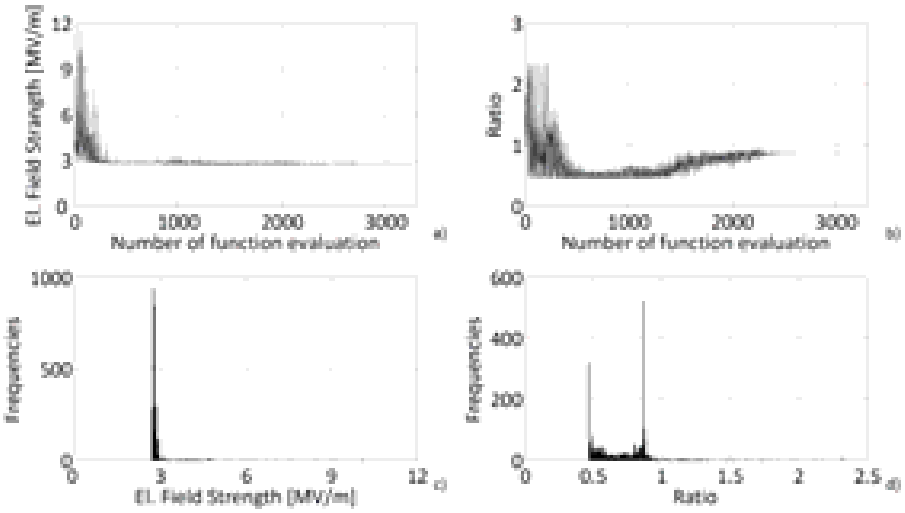

Fig. 8: *a) Electrical field strength/iteration b) Ratio of electrical field strength values/iteration c) The electrical field strength histogram d) The ratio histogram.*

4 CONCLUSION

A pre-processor that supports the parametrical entry of a model has been made using MATLAB. It enables, together with a mesh generator, numerical calculation with FEM and an optimization algorithm, a quick and reliable modeling of insulating elements. Parametrical entry enables the employment of different optimization algorithms and the testing of different bushing versions within a short period of time as well. One of these was the covering of a shield with different dielectric material than the material of the bushing body. Insertion of the additional dielectric material led us to a two different objectives, which were in conflict with each other. These objectives were merged into a single one using the weighting of objectives technique. In our case, a greater weight was given to the minimum objective function $f_E(\boldsymbol{x})$, which meant that a greater emphasis was given to a lowering of electrical field strength value around a bushing. A known problem of this technique is that even slightly modifying weights can lead an algorithm to a non-converging state. Furthermore, the change of the objectives priority requires new run of the modeling algorithm.

References

[1] **Pihler, J.**: *Switchgear of electric power system*, University of Maribor, Faculty of Electrical Engineering and Computer Science, 2003

[2] **Kitak, P., Pihler, J., Ticar, I.**, *Optimization algorithm for the design of bushing for indoor SF6 switchgear applications*, *IEE proc., Gener. transm. distrib.*, vol. 152, pp. 691-696, 2005

[3] Program tools ELEFANT: Institute for Fundamentals and Theory in Electrical Engineering, University of Technology. Graz, 2000

[4] **Storn, R., Price, K.:** *Minimizing the real functions of the ICEC'96 contest by differential evolution, in Proc. of ICEC96*, pp. 842-844, 1996

JET Volume 2 (2009), p.p. 65 - 74

Issue 2, June 2009

www.fe.uni-mb.si/JET

AXIAL-FLUX PERMANENT MAGNET SYNCHRONOUS GENERATORS FOR WIND TURBINE APPLICATIONS

SINHRONSKI GENERATORJI S TRAJNIMI MAGNETI IN AKSIALNIM MAGNETNIM PRETOKOM ZA VETRNE TURBINE

P. Virtičℜ, P. Pišek, B. Štumberger, M. Hadžiselimović, T. Marčič

Keywords: analytical method, electric machines, finite element method, magnetic field, permanent magnet generators, synchronous generators, wind turbine generators

Abstract

This paper presents an axial-flux permanent magnet generator (AFPMSG) with coreless stator for wind turbine applications. In the introduction of this paper, a survey of existent wind turbine generators with regards to their advantages and disadvantages is presented. An overview of generators is based on many wind generator systems built during previous decades, which are still in operation. In recent years, the technologies for exploiting the wind energy have rapidly developed and a variety of wind generator systems is available today on the global market. The selection of appropriate wind generator system mainly depends on the user demands, operating conditions, level of production difficulty and costs. Further, the dependencies between geometrical design and characteristics of coreless stator AFPMSG are presented. Due to the absence of cogging torque, the coreless stator AFPMSG is a very useful generator design, especially at low wind speeds.

ℜ Corresponding author: Peter Virtič, Tel.: +386-2-333-1350, Fax: +386-2-333-1351, Mailing address: TECES, Pobreška cesta 20, 2000 Maribor E-mail address: peter.virtic@uni-mb.si, peter.virtic@gmail.com

---

Povzetek

V članku je predstavljen sinhronski generator s trajnimi magneti in aksialnim magnetnim pretokom brez železnega jedra statorja za vetrne turbine. Uvodoma je podan pregled obstoječih generatorjev za vetrne turbine, pri čemer so na kratko predstavljene njihove prednosti in slabosti. Pregled generatorskih sistemov je prilagojen dejstvu, da je bilo v zadnjih desetletjih zgrajeno zelo veliko vetrnih generatorskih sistemov, ki obratujejo še danes. V zadnjih letih se tehnologije izkoriščanja energije vetra hitro razvijajo, zato imamo na voljo precejšnjo izbiro generatorskih sistemov, katerih izbira je odvisna predvsem od zahtev, pogojev obratovanja, zahtevnosti izdelave ter stroškov. V nadaljevanju je podrobno predstavljena odvisnost karakteristik od geometrijskih parametrov za sinhronski generator s trajnimi magneti in aksialnim magnetnim pretokom brez železnega jedra statorja, ki se zaradi odsotnosti samozadržnega vrtilnega momenta izkaže za dobro izbiro, zlasti pri nizki hitrosti vetra.

1 INTRODUCTION

With the rapid development of wind power technologies, various wind turbine and generator concepts have been developed. Wind turbine generators are somewhat different from conventional generators, because they have to operate with the wind turbine rotor, which supplies highly fluctuating mechanical power.

Wind turbines can be designed with either synchronous or induction generators, which can be directly or indirectly connected to the grid. With direct grid connection, the generator is connected directly to the alternating current grid. In contrast, with an indirect grid connection, the three-phase current from the generator usually passes through a series of electric devices that adjust the electrical current and/or voltage level to match that of the grid.

With regards to rotational speed, the wind generator systems can be divided into three groups: fixed speed, limited variable speed and variable speed [1]. The fixed speed wind generator systems usually consist of a multiple-stage gearbox and squirrel-cage induction generator with capacitors for reactive power compensation. Its well-known advantages are robustness, simplicity and cheap mass production. In contrast, the squirrel-cage induction generator is directly connected to the grid and operates only in a narrow range above the synchronous speed. For this reason, the turbine speed cannot be adjusted with the wind speed to optimize the aerodynamic efficiency. Another disadvantage of the squirrel-cage induction generator is its inability to support grid voltage control due to the necessary excitation current obtained from the grid. These generators cannot provide continuous speed variations. The speed level can be changed only by using pole-changeable induction generator and multi-stage gearbox with large mass and high costs. The limited variable speed wind generator systems usually consist of a multiple-stage gearbox and wound rotor induction generator with variable rotor resistance using a power electronic converter. The stator of wound rotor induction generator is directly connected to the grid. By changing the rotor resistance, the rotational speed can be continuously increased above the synchronous speed, but the speed limit is still too low.

The variable speed wind generator systems with partial-scale power converters usually include a multiple-stage gearbox and wound rotor induction generator [12]. This generator system is known as the doubly fed induction generator, where the stator is directly connected to the grid, whereas the rotor is connected to the grid through the power converter, which controls the rotor frequency. The variable speed range above the synchronous speed is increased and the

rotor energy can be transmitted through the converter into the grid instead of being dissipated. Despite many other advantages of doubly fed induction generators, such as efficient reactive power compensation, smooth grid connection, voltage support towards the grid, it has also many disadvantages, including slip rings, large currents under grid fault conditions and usually complicated control strategies. The multi-stage gearbox is necessary, because the speed range is still far from a common turbine speed.

The variable speed wind generator systems with full-scale power converters can be gearless, single-stage geared or multi-stage geared, and with a full-scale power converter connecting the generator to the grid. Gearless generator systems usually include generators with a large diameter and small pole pitch; they have high overall efficiency, reliability and availability without gearbox. Types of gearless (direct-drive) generators available on the market can be classified into electrically excited synchronous generators and permanent magnet (PM) synchronous generators [2, 4, 9]. PM synchronous generators can be, according to the magnetic flux direction, further classified into radial flux (see Figure 1a) and axial flux generators (see Figure 1b). An axial-flux permanent magnet synchronous generator (AFPMSG) with coreless stator is the main focus of this paper.

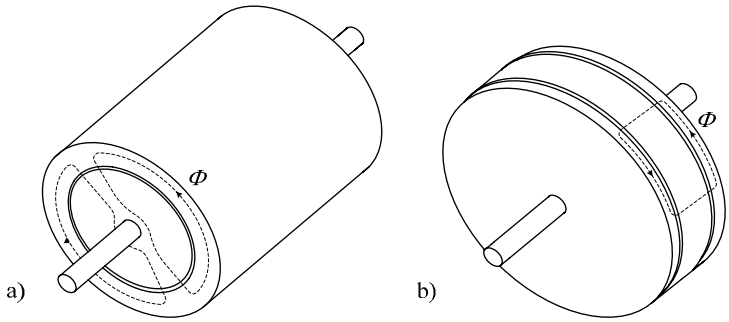

Figure 1: *Two basic topologies of PM synchronous generators according to the main magnetic flux direction: a) radial flux generator, b) axial flux generator.*

Radial flux PM generators for direct-drive wind turbines can operate with a good performance over a wide range of rotational speeds and usually with higher torque density than electrically excited synchronous generators.

In the variable speed single-stage geared wind generator systems with full-scale power converters, the single-stage gearbox connects the wind turbine and low speed PM generator. In contrast, the variable speed multi-stage geared wind generator systems with full-scale power converters need large and expensive power converters and are classified into PM synchronous and squirrel-cage induction wind generator systems.

The maximum torque that generators can handle depends on the rotor volume. For a desired power output, the choice between a slow-moving, large and expensive generator and a high-speed, smaller and cheaper generator is given. It is a very useful mechanical property that the induction generator increases or decreases its speed slightly with the torque variations. This is one of the most important reasons when using an induction generator rather than a synchronous generator as a wind turbine generator, which is directly connected to the electrical grid.

A PM synchronous generator can run without connection to the public grid. However, the stator of an induction generator has to be magnetized from the grid before it operates. Alternatively, an induction generator can operate in a stand-alone system, if the necessary magnetization current is provided with capacitors. It also requires remanence in the rotor iron, which can be leftover from previous generator operation.

Besides the fundamental generator systems mentioned above, many other systems are also presented in the literature [3, 7].

The advantages of AFPMSGs in comparison with radial flux PM synchronous generators are as follows: simple winding, low noise and cogging torque in slotless generators, short axial length and higher torque density. In contrast, the disadvantages are larger outer diameter, large amount of PMs in slotless generators, difficult maintenance of air-gap on large diameter, difficult production of stator core for slotted generators.

In this paper, the comparison of static characteristics for coreless stator AFPMSG with different coil and pole numbers is presented. Moreover, the best "number of coils/number of poles" combination is selected from among eight calculated topologies.

2 AXIAL FLUX PERMANENT MAGNET SYNCHRONOUS GENERATORS

Three basic configurations of AFPMSGs exist, with regards to the number and positions of stators and rotors, which are standing and moving generator parts, respectively (see Figure 2).

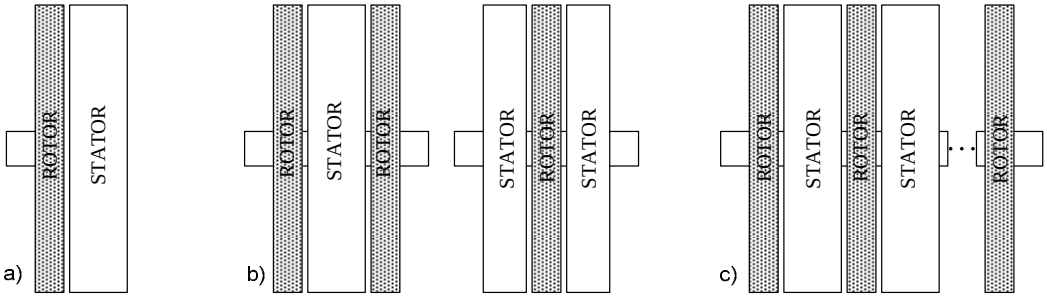

Figure 2: *Basic configurations of AFPMSGs: a) single-sided, b) double-sided, c) multi-disc.*

AFPMSGs consist of slotted or non-slotted stators and rotors with PMs [5]. Both, stator and rotor core of the single-sided AFPMSG (see Figure 2a) usually needs a ferromagnetic material to complete the magnetic circuit. Stator cores are usually formed from laminated or powdered iron, such as soft magnetic composites [6, 8, 10] in order to reduce eddy currents and consequently iron losses. The same approach has to be used to design a stator core of double-sided AFPMSG with double external stator and single internal rotor.

Alternatively, AFPMSGs with double external rotors can be designed with an ironless internal stator. Due to the absence of stator iron losses, the AFPMSGs with non-ferromagnetic (coreless) stators usually operate at higher efficiency in comparison with the generators with ferromagnetic stator cores. However, more PM material is needed to keep an acceptable level of magnetic flux density along the stator thickness (d_s). Combining single and double-sided AFPMSGs (see Figure 2b) on the same shaft, a multi-disc machine is obtained (see Figure 2c).

The manufacturing process of a laminated stator core is comprehensive and expensive. The slots can be punched before or milled after the steel strip is rolled into the laminated core. Powdered soft magnetic materials partially simplify the manufacturing process and costs of stator cores with compound shapes. Powder metallurgy uses a sintering process for making various parts out of metal powder.

By increasing the wind speed and, thereby the rotational speed of the AFPMSG, the output generator power increases. One very important wind generator characteristic is the ability to also produce electrical energy at low wind velocities. The construction of PM synchronous generators with ferromagnetic stator core can cause cogging torque problems. Cogging torque is an inherent characteristic of PM generators and is caused by the geometry of the generator. It affects the self-start ability at low wind velocity, produces noise and, together with other mechanical tensions [11], causes mechanical vibrations which shorten the lifespan of mechanical devices. For this reason, minimizing cogging torque is important in improving the operation of wind turbines.

AFPMSGs with coreless stators have no cogging torque and are designed to be simple and efficient with fast and easy construction. The coreless stator AFPMSG analyzed in this paper consists of an internal stator and twin external rotors. PMs are glued to the rotor steel discs and the coils are built into the nonmagnetic stator supporting structure. The AFPMSG excitation is accomplished by using Neodymium-Ferrum-Boron (NdFeB) PMs on the both parts of the double rotor. Design parameters of the active part of double-sided AFPMSG with coreless internal stator are presented in Figure 3.

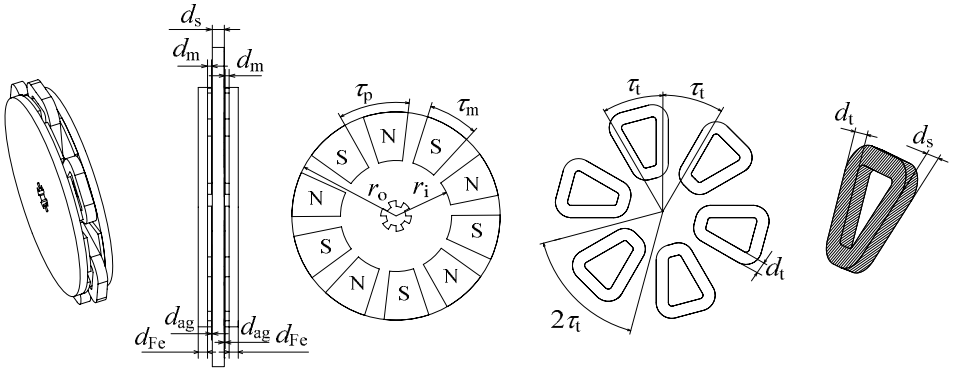

Figure 3: *Design parameters of AFPMSG with 10 poles and 6 coils.*

3 ANALYSIS OF AFPMSG WITH RESULTS AND DISCUSSION

Coreless stator AFPMSG characteristics are analytically calculated for several “number of coils/number of poles” combinations. Within the particular combination, the influence of the design parameters can be analyzed. The design procedure is iterative in order to obtain appropriate characteristics with regards to initial specifications of wind generator. For this reason, the comparisons between different “number of coils/number of poles” combinations are presented. In order to assure comparable results for the different combinations, the design parameters remain constant if possible. By changing the number of coils, the coil side width (d_t) and the number of turns (N) change at a constant amount of stator copper (see Figure 5). Stator

---

winding of the analyzed coreless stator AFPMSG consists of two partial windings (N=*2x50*) which are placed symmetrically on the each side of the supporting nonmagnetic stator structure. By changing the number of poles, the angle of nonmagnetic region between two adjacent PMs is constant. Figure 4 presents the back electromotive force (back EMF) according to displacement for different number of poles at six stator coils. A static torque comparison for the same combinations is presented in Figure 6 and shows that the combination with six coils and 10 poles, with the same amount of copper, is the most appropriate.

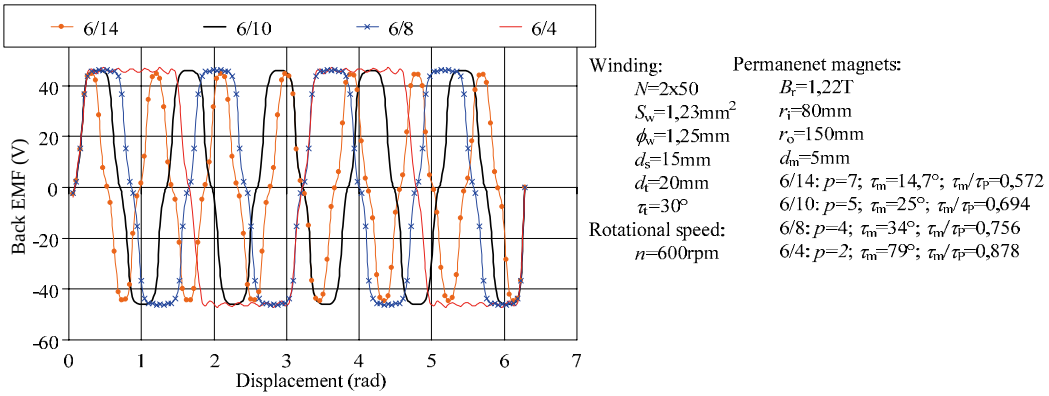

Figure 4: *Comparison of back EMF according to displacement for different "number of coils/number of poles" combinations.*

The amplitude of back EMF does not change according to the number of poles due to the constant winding parameters. By reducing the number of turns by one third at the same time when the number of coils increases by one third, the back EMF amplitude remains constant at different pole numbers (see Figure 5).

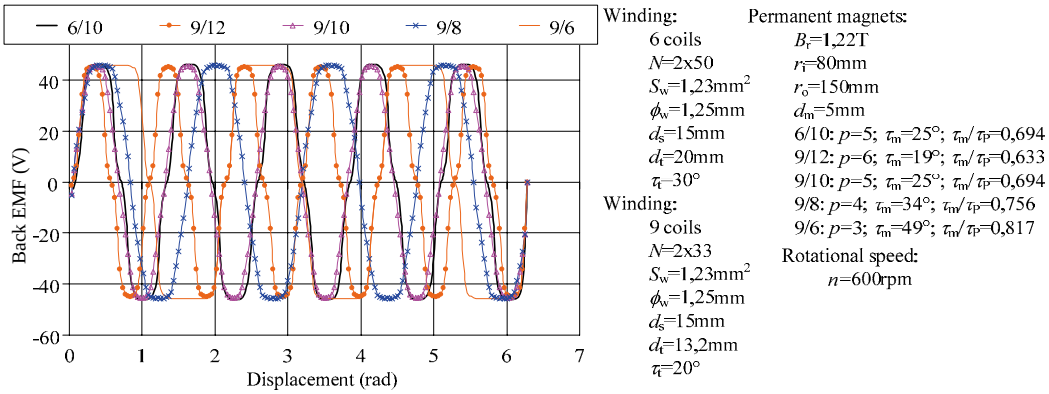

Figure 5: *Comparison of back EMF according to displacement for different "number of coils/number of poles" combinations.*

Figure 7 shows that the best combination is still six coils and 10 poles; although the combinations with nine coils are closer than the other combinations of poles with six coils (see Figure 6).

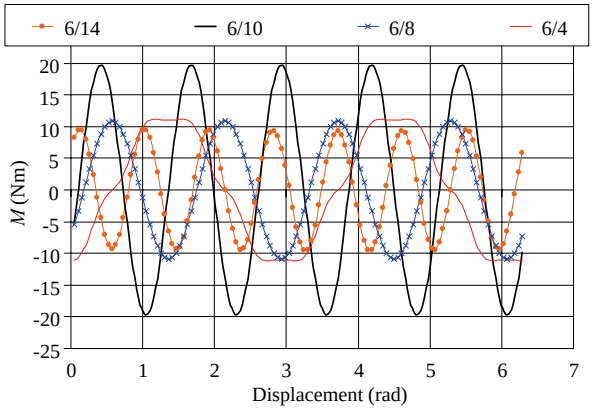

Winding:
N=2x50
J_{cu}=5A/mm^2
I=2x6,15A
S_w=1,23mm^2
ϕ_w=1,25mm
d_s=15mm
d_t=20mm
τ_t=30°

Permanent magnets:
B_r=1,22T
r_i=80mm
r_o=150mm
d_m=5mm
6/14: p=7; τ_m=14,7°; τ_m/τ_p=0,572
6/10: p=5; τ_m=25°; τ_m/τ_p=0,694
6/8: p=4; τ_m=34°; τ_m/τ_p=0,756
6/4: p=2; τ_m=79°; τ_m/τ_p=0,878

Figure 6: *Comparison of static torque according to displacement for different "number of coils/number of poles" combinations.*

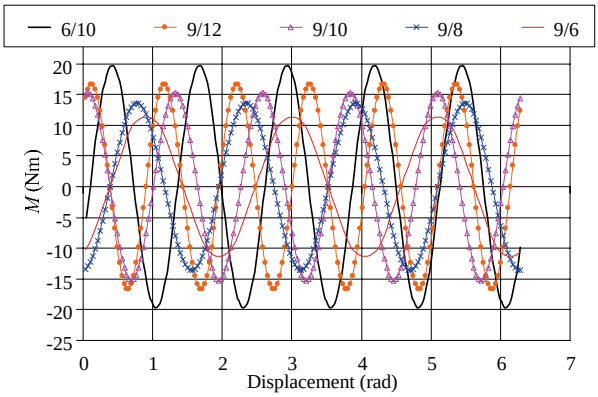

Winding:
J_{cu}=5A/mm^2
I=2x6,15A
S_w=1,23mm^2
ϕ_w=1,25mm
d_s=15mm
6 coils:
N=2x50
d_t=20mm
τ_t=30°
9 coils:
N=2x33
d_t=13,2mm
τ_t=20°

Permanent magnets:
B_r=1,22T
r_i=80mm
r_o=150mm
d_m=5mm
6/10: p=5; τ_m=25°; τ_m/τ_p=0,694
9/12: p=6; τ_m=19°; τ_m/τ_p=0,633
9/10: p=5; τ_m=25°; τ_m/τ_p=0,694
9/8: p=4; τ_m=34°; τ_m/τ_p=0,756
9/6: p=3; τ_m=49°; τ_m/τ_p=0,817

Figure 7: *Comparison of static torque according to displacement for different "number of coils/number of poles" combinations.*

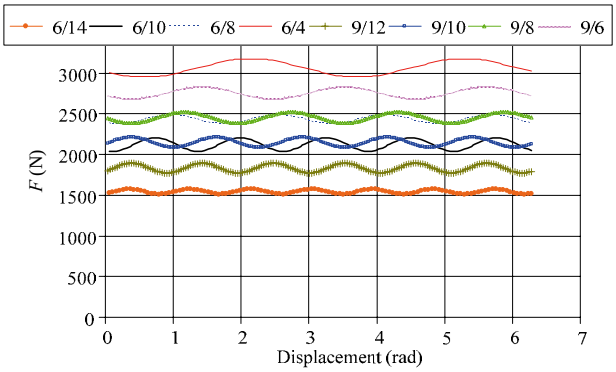

Winding:
J_{cu}=5A/mm^2
I=2x6,15A
S_w=1,23mm^2
ϕ_w=1,25mm
d_s=15mm
6 coils:
N=2x50
d_t=20mm
τ_t=30°
9 coils:
N=2x33
d_t=13,2mm
τ_t=20°

Permanent magnets:
B_r=1,22T
r_i=80mm
r_o=150mm
d_m=5mm
6/14: p=7; τ_m=14,7°; τ_m/τ_p=0,572
6/10: p=5; τ_m=25°; τ_m/τ_p=0,694
6/8: p=4; τ_m=34°; τ_m/τ_p=0,756
6/4: p=2; τ_m=79°; τ_m/τ_p=0,878
9/12: p=6; τ_m=19°; τ_m/τ_p=0,633
9/10: p=5; τ_m=25°; τ_m/τ_p=0,694
9/8: p=4; τ_m=34°; τ_m/τ_p=0,756
9/6: p=3; τ_m=49°; τ_m/τ_p=0,817

Figure 8: *Comparison of attractive force between rotor discs according to displacement for different "number of coils/number of poles" combinations.*

Figure 8 presents the comparison of attractive force between the rotor discs for combinations with both six and nine coils in the stator winding. By increasing the number of poles, the attractive force decreases.

4 CONCLUSION

Static torque, back EMF and attractive force characteristics are calculated by using analytical method of magnetic field calculation, which has already been validated in [13] by means of finite elements method and measurements on prototype AFPMSG. Static torque and attractive force are calculated using the Maxwell stress tensor method, whereas the back EMF is calculated considering the time variation of magnetic flux within each stator coil, where the magnetic flux is calculated by integrating the magnetic vector potential along the closed contour, which is placed at the centre of the coil side width (d_t) on the one fourth of the stator width (d_s). Due to the concentrated winding, which causes the limited options for the coil side connections, the combination with six coils and 10 poles is the most appropriate among the calculated AFPMSGs.

References

[1] **Li, H., Chen, Z.:** *Overview of different wind generator systems and their comparisons,* IET Renewable Power Generation, vol. 2, issue 2, June 2008, pp. 123-138.

[2] **Chen, Y., Pillay, P., Khan, A.:** *PM wind generator topologies,* IEEE Transactions on Industry Applications, vol. 41, issue 6, Nov.-Dec. 2005, pp. 1619-1626.

[3] **Liu, X., Lin, H., Zhu, Z. Q., Yang, C., Fang, S., Guo, J.:** *A Novel Dual-Stator Hybrid Excited Synchronous Wind Generator,* IEEE Transactions on Industry Applications, vol. 45, issue 3, May-Jun. 2009, pp. 947-953.

[4] **Yang, G., Li, H.:** *Design and analysis of a newly brushless DC wind generator,* World Automation Congress 2008, Sep.-Oct. 2008, pp. 1-5.

[5] **Parviainen, A., Pyrhonen, J., Kontkanen, P.:** *Axial Flux Permanent Magnet Generator with Concentrated Winding for Small Wind Power Applications,* IEEE International Conference on Electric Machines and Drives 2005, May 2005, pp. 1187-1191.

[6] **Chen, Y., Pillay, P.:** *Axial-flux PM wind generator with a soft magnetic composite core,* Conference Record of the Industry Applications Conference 2005, vol. 1, Oct. 2005, pp. 231-237.

[7] **Rahman, M.A.:** *Advances of interior permanent magnet (IPM) wind generators,* International Conference on Electrical Machines and Systems 2008, ICEMS 2008, Oct. 2008, pp. 2228-2233.

[8] **Khan, M.A., Dosiek, L., Pillay, P.:** *Design and Analysis of a PM Wind Generator with a Soft Magnetic Composite Core,* IEEE International Symposium on Industrial Electronics 2006, vol. 3, Jul. 2006, pp. 2522-2527.

[9] **Yu, S. Xue, Han, L., Li, H., Li-D. Xie:** *Optimal design and comparison of different PM synchronous generator systems for wind turbines,* International Conference on Electrical Machines and Systems 2008, ICEMS 2008, Oct. 2008, pp. 2448-2453.

---

[10] **Khan, M.A., Pillay, P., Batane, N.R., Morrison, D.J.:** *Prototyping a Composite SMC/Steel Axial-flux PM Wind Generator,* Conference Record of the IEEE Industry Applications Conference 2006, vol. 5, Oct. 2006, pp. 2374-2381.

[11] **Gregorc, B., Predin, A.:** *Comparison of measurement shaft displacement, bearing casing vibrations and axial forces in three different Kaplan turbines, Journal of Energy Technology*, vol. 2, issue 1, Mar. 2009, pp. 9-24.

[12] **Li, H., Chen, Z.:** *Design Optimization and Evaluation of Different Wind Generator Systems,* International Conference on Electrical Machines and Systems 2008, ICEMS 2008, Oct. 2008, pp. 2396-2401.

[13] **Virtič, P., Pišek, P., Marčič, T., Hadžiselimović, M., Štumberger, B.:** *Analytical analysis of magnetic field and back electromotive force calculation of an axial-flux permanent magnet synchronous generator with coreless stator,* IEEE Transactions on Magnetics, vol. 44, issue 11, Nov. 2008, pp. 4333-4336.

Nomenclature

(Symbols)	(Symbol meaning)
B_{r}	remanent magnetic flux density
d_{t}	coil side width
d_{s}	stator and coil side thickness
d_{Fe}	rotor iron thickness
d_{ag}	air-gap thickness
d_{m}	PM thickness
F	electromagnetic force
I	electric current
J_{Cu}	electric current density
M	electromagnetic torque
N	number of turns
p	pole pair number
r_{o}	outer radius of PM
r_{i}	inner radius of PM
S_{w}	copper wire cross section
Φ_{w}	copper wire diameter
τ_{t}	coil pitch
τ_{p}	pole pitch
τ_{m}	angle of PM

---

www.fe.uni-mb.si/JET

AUTHOR INSTRUCTIONS (MAIN TITLE)

SLOVENIAN TITLE

Authors, Corresponding author[ℜ]

Key words: (Up to 10 keywords)

Abstract

Abstract should be up to 500 words long, with no pictures, photos, equations, tables, only text.

Povzetek

(In Slovenian language)

Submission of Manuscripts: All manuscripts must be submitted in English by e-mail to the editorial office at JET-editors@uni-mb.si to ensure fast processing. Instructions for authors are also available online at www.fe.uni-mb.si/JET .

Preparation of manuscripts: Manuscripts must be typed in English in prescribed journal form (Word editor). A Word template is available at the Journal Home page.

A title page consists of the main title in the English and Slovenian languages; the author(s) name(s) as well as the address, affiliation, E-mail address, telephone and fax numbers of author(s). Corresponding author must be indicated.

Main title: should be centred and written with capital letters (ARIAL **bold** 18 pt), in first paragraph in English language, in second paragraph in Slovenian language.

Key words: A list of 3 up to 6 key words is essential for indexing purposes. (CALIBRI 10pt)

Abstract: Abstract should be up to 500 words long, with no pictures, photos, equations, tables, - text only.

Povzetek: - Abstract in Slovenian language.

[ℜ] Corresponding author and other authors: Title, Name and Surname, Tel.: +XXX x xxx xxx, Fax: +XXX x xxx xxx, Mailing address: xxxxxxxxxxxxxxxxxxxxxxxxxxxxxxxxx, E-mail address: email@xxx.xx

---

Main text should be structured logically in chapters, sections and sub-sections. Type of letters is Calibri, 10pt, full justified.

Units and abbreviations: Required are SI units. Abbreviations must be given in text when firstl mentioned.

Proofreading: The proof will be send by e-mail to the corresponding author, who is required to make their proof corrections on a print-out of the article in pdf format. The corresponding author is responsible to introduce corrections of data in the paper. The Editors are not responsible for damage or loss of manuscripts submitted. Contributors are advised to keep copies of their manuscript, illustrations and all other materials.

The statements, opinions and data contained in this publication are solely those of the individual authors and not of the publisher and the Editors. Neither the publisher nor the Editors can accept any legal responsibility for errors that could appear during the process.

Chapter examples:

1 MAIN CHAPTER

(Arial bold, 12pt, after paragraph 6pt space)

1.1 Section

(Arial bold, 11pt, after paragraph 6pt space)

1.1.1 Sub-section

(Arial bold, 10pt, after paragraph 6pt space)

Example of Equation (lined 2 cm from left margin, equation number in normal brackets (section.equation number), lined right margin, paragraph space 6pt before in after line):

$$c = \sqrt{a^2 + b^2} \tag{1.1}$$

Tables should have a legend that includes the title of the table at the top of the table. Each table should be cited in the text.

Table legend example:

Table 1: *Name of the table (centred, on top of the table)*

Figures and images should be labelled sequentially numbered (Arabic numbers) and cited in the text. The legend should be below the image, picture, photo or drawing.

Figure legend example:

Figure 1: *Name of the figure (centred, on bottom of image, photo, or drawing)*

References

[1] **Name. Surname:** *Title,* Publisher, p.p., Year of Publication

Example of reference-1 citation: In text, Predin, [1], text continue. **(Reference number order!)**

JET

JET Journal of ENERGY TECHNOLOGY Vol. 2/2 2009 UNIVERSITY OF MARIBOR, FACULTY OF ENERGY TECHNOLOGY

9 771855 574008

ISSN 1855-5748